Title: Systematic characterization of brain cellular crosstalk signaling networks in Alzheimer's disease reveals a novel role for SEMA6D in TREM2-dependent microglial activation

Authors: Ricardo D'Oliveira Albanus[1,2,3]*, Gina M. Finan[4,5]*, Logan Brase[1,2,3], Shuo Chen[6], Qi Guo[7], Abhirami Kannan[1,2,3], Mariana Acquarone[1,2,3], Shih-Feng You[1,2,3], Brenna C Novotny[1,2,3], Patricia M Ribeiro Pereira[8], John C Morris[2,9,10,11], Eric McDade[1,11], Carlos Cruchaga[1,2,3,11], Jasmeer P Chhatwal[11,12], Dominantly Inherited Alzheimer Network (DIAN)[11], Emily E Mace[13], Bruno A Benitez[14], Laura Piccio[2,15,16], Greg T Sutherland[17], Qin Ma[7], Hongjun Fu[6], Celeste M Karch[1,2,3,11], Oscar Harari[1,2,3†], Tae-Wan Kim[4,5†]

[1]Department of Psychiatry, Washington University School of Medicine, St. Louis, MO, USA
[2]Hope Center for Neurological Disorders, Washington University School of Medicine, St. Louis, MO, USA
[3]NeuroGenomics and Informatics, Department of Psychiatry Washington University in St. Louis
[4]Department of Pathology and Cell Biology, Columbia University Irving Medical Center, New York, NY, USA
[5]Taub Institute for Research on Alzheimer's Disease and the Aging Brain, Columbia University Irving Medical Center, New York, NY, USA
[6]Department of Neuroscience, The Ohio State University Wexner Medical Center, Columbus, OH, USA
[7]Department of Biomedical Informatics, Ohio State Comprehensive Cancer Center, Columbus, OH, USA
[8]Department of Radiology, Division of Radiological Sciences, Washington University School of Medicine, St. Louis, MO, USA
[9]Knight Alzheimer Disease Research Center, Washington University School of Medicine, St. Louis, MO, USA
[10]Department of Neurology, Washington University School of Medicine, St. Louis, MO, USA
[11]Dominantly Inherited Alzheimer Network (DIAN)
[12]Department of Neurology, Massachusetts General Hospital, Harvard Medical School, Boston, MA, USA
[13]Department of Pediatrics, Columbia University, New York, NY, USA
[14]Department of Neurology, Beth Israel Deaconess, Harvard Medical School, Boston, MA, USA
[15]Department of Pathology and Immunology, Washington University School of Medicine, St. Louis, MO, USA
[16]Brain and Mind Centre, School of Medical Sciences, University of Sydney, Camperdown, NSW, Australia
[17]School of Medical Sciences and Charles Perkins Centre, Faculty of Medicine and Health, The University of Sydney, Sydney, NSW, Australia

*** Contributed equally**

[†] **Corresponding authors**

Abstract

Disrupted cross-cellular communication signaling (cellular crosstalk) has been implicated in neurodegenerative diseases, including Alzheimer's disease (AD). However, there is currently no systematic characterization of brain crosstalk networks in health and disease. We systematically characterized brain cellular crosstalk networks using single-nucleus transcriptomics data from a large cohort of control and AD brain donors (n=67). We found that crosstalk interactions between microglia and neurons were highly enriched to directly involve reported AD risk genes as ligands or receptors. Computational reconstruction of the co-expression networks associated with neuron-microglia crosstalk revealed they perturb additional known AD risk genes in microglia. We identified the interaction of neuronal SEMA6D (a PLXNA1 ligand) with a highly connected microglial regulatory sub-network involving *TREM2*, *APOE*, and *HLA* genes, which we predict is disrupted in late AD stages. Using CRISPR-modified human induced pluripotent stem cell (iPSC)-derived microglia and treatment with recombinant SEMA6D, we experimentally demonstrated that SEMA6D promotes microglial phagocytosis and cytokine (TNFα and IL-6) release in a TREM2-dependent manner. The novel discovery that the SEMA6D-PLXNA1/TREM2 signaling axis is involved in the regulation of microglia function demonstrates that our systematic characterization of cellular crosstalk networks is an important strategy for discovering specific mediators of significant cross-cellular interactions important to AD pathogenesis, gaining wider insights into the biology of this disease, and uncovering novel therapeutics.

Introduction

Cross-cellular signaling (cellular crosstalk) is integral to brain function. By establishing cellular networks mediated by membrane receptors and their corresponding ligands, cells can gather information from their immediate environment and respond accordingly. Cellular crosstalk is crucial to brain homeostasis and crucial processes of neurodevelopment, particularly for synaptic pruning and axon guidance (*1*, *2*). However, increasing experimental and genetic evidence implicates aberrant crosstalk in neurodegenerative diseases (*3*–*5*). For instance, a recent study systematically characterized crosstalk interactions involving astrocytes and microglia in a mouse model of multiple sclerosis and identified a role for the plexin, semaphorin, and ephrin protein families in neuroinflammation (*5*). Similarly, another study identified a role for astrocyte-microglia crosstalk in modulating amyloid pathology (*6*), and other studies highlighted the role of plexin-semaphorin signaling in mediating immune responses in microglia and other myeloid cells (*7*, *8*). These findings indicate that aberrant cellular crosstalk interactions likely contribute to neurodegeneration. From a translational view, cellular crosstalk is an attractive molecular target for drug development, as s membrane receptors have been widely studied as better therapeutic targets (*9*–*11*).

Genome-wide association studies have successfully identified genetic risk factors for Alzheimer's disease (AD) and the gene products likely to mediate these signals (*12*–*15*). Functional genomics leveraging human tissue (*16*–*19*) and experimental data from human induced pluripotent stem cell (iPSC)-derived cells (*20*) identified a significant fraction of AD risk genes expressed by microglial cells. However, how are the AD risk genes modulated is still unknown. Microglia are the resident immune cells in the brain and are highly attuned to their

surrounding environment sensing signals from neighboring cells (*21*). Therefore, we hypothesized that microglial AD risk genes modulate cellular crosstalk between microglia and other brain cell types.

In this study, we used single-nucleus transcriptomic profiles from neuropath-free controls and AD human brains across a broad spectrum of neuropathological states and genetic backgrounds to systematically reconstruct the cellular crosstalk networks across seven major brain cell types: microglia, astrocytes, oligodendrocytes, oligodendrocytes precursors (OPC), excitatory (exc.) and inhibitory (inh.) neurons, and endothelial cells. We found that neuron-microglia crosstalk interactions were highly enriched compared to other cross-cellular interactions to directly involve known AD risk genes. In addition, we identified a sub-network of microglial genes centered around *TREM2*. We predict this subnetwork is disrupted in late-stage AD and modulated by the crosstalk interaction between neuronal semaphorin 6D (SEMA6D) and microglial TREM2. Interestingly, SEMA6D is a known ligand of Plexin-A1, which interacts with TREM2 and TYROBP (DAP12) to form a receptor complex(*7*). Semaphorins and their receptors regulate immune cell function and are genetically and functionally implicated in AD (*6*, *22–24*). Using wild-type (WT) and *TREM2* knockout (KO) iPSC-derived microglia (iMGL), we showed that SEMA6D promotes microglia functions, including phagocytosis and cytokine release in a TREM2-dependent manner. Our findings demonstrate that systematic characterization of cellular crosstalk networks in human brains is a viable strategy to elucidate aberrant regulatory biology in AD and other neurodegenerative diseases.

Results

Analyses of human brain transcriptomic profiles identify a role for cellular crosstalk in AD

To systematically characterize cellular crosstalk interactions in neuropath-free controls and AD brains, we analyzed single-nucleus transcriptomic profiles (snRNA-seq) of superior parietal cortex tissue samples from donors of the Knight Alzheimer Disease Research Center (Knight ADRC) and the Dominantly Inherited Alzheimer Network (DIAN) (*16*). This dataset encompasses different AD subtypes, including sporadic AD and autosomal dominant AD, with donors distributed in a broad spectrum of neuropathological states and genetic backgrounds, including carriers of *TREM2* risk variants **(Figure 1a, Supp. Table 1)**. We identified patterns of ligand-receptor gene expression across cell type pairs and their corresponding transcriptional states using CellPhoneDB (*25*), which has been successfully used to predict patterns of cellular crosstalk. We performed the analyses to detect condition-specific crosstalk interactions by stratifying brains by disease status and genetic group. In total, we identified between 961 and 1,600 (median 1,521) significant (Bonferroni-corrected $p < 0.05$) crosstalk interactions between cellular state pairs across all donor categories **(Figure 1b; Supp. Figure 1a; Supp. Table 2**). Furthermore, the observed crosstalk patterns were highly robust to dataset downsampling, including removing a subset of donors and using 100 barcodes or less per transcriptional state (fraction of replication 0.81 to 0.86 across donor categories, median = 0.84; **Supp. Figure 1b-c**). These results indicate that the crosstalk interaction patterns identified using CellPhoneDB were not driven by technical factors such as the number of donors, nuclei, and barcode sequencing depth.

We compared the crosstalk patterns across donor categories to identify AD-related global changes. Overall, crosstalk interactions involving microglia were significantly increased in all AD donors compared to controls (OR=1.21, adj. p=5.22e-4), and we detected a significant decrease in crosstalk involving excitatory neurons in sporadic AD donors (OR = 0.82, adj. p=0.03; **Supp. Figure 2**). These results are consistent with neuronal loss and the critical role of microglia in AD onset. We next performed a functional enrichment of the genes associated with the up- and down-regulated crosstalk interactions in each cell type to determine the biological pathways perturbed in AD. Consistent with significant changes in cellular homeostasis in AD brains, we observed changes in the cellular crosstalk patterns between neuropath-free control and AD donors. The crosstalk interactions up-regulated in AD were significantly enriched for pathways indicative of immune activation and cellular stress (**Figure 1c**). Interestingly, we observed a significant increase in ephrin signaling in autosomal dominant AD donors (p = 1.48e-12). This finding agrees with the previously described role of this signaling pathway in neuroinflammation and neurodegeneration (*5*). Aiming to understand how each cell type likely contributes to AD crosstalk, we also performed a similar functional enrichment analysis focusing on cell types to identify crosstalk interactions changed in AD. We observed a potential role for multiple cell types contributing to immune activation and neuronal stress (**Supp. Figure 3**). Together, these results indicate that AD involves widespread dysregulation of homeostatic cross-cellular signaling pathways.

Our initial analysis identified thousands of significant crosstalk interactions across all cell types and donor categories. We next sought to focus on interactions involving genes linked to AD by genetic and functional studies, which we hypothesized were more likely to be early drivers of AD. (**Supp. Table 3**). We identified 90 crosstalk interactions directly involving an AD gene as either the ligand or receptor, of which 34 were considered significant by CellPhoneDB in at least one cell type pair (**Figure 1d**). Microglia had the highest enrichment for crosstalk interactions involving AD genes ($\log_2$ OR range: 0.85 to 1.76, median = 1.23, *p* range: 4.69e-3 to 3.08e-8, median = 2.68e-4; **Figure 1e**), and most of these interactions (64.9%) involved microglia as the likely receptor cell type. These enrichment patterns were robust to the observed increase in the number of crosstalk interactions involving microglia in AD vs. controls and the overall higher representation of AD genes in microglia (**Supp. Figure 4**, Methods).

We next analyzed which cell type(s) were most likely to interact with microglia crosstalk by conditioning the previous analyses on microglia. We observed that excitatory neurons had the highest enrichment point estimates to partner with microglia for crosstalk interactions involving AD genes mainly due to pre-symptomatics ($\log_2$ OR = 1.98, p = 0.035; **Figure 1f**). We replicated these analyses in three case-control snRNA-seq datasets of the prefrontal cortex region from the South West Dementia Brain Bank (SWDBB), the Rush ADRC, and the University of California Irvine Institute for Memory Impairments and Neurological Disorders (UCI MIND) ADRC (**Supp. Table 4**) (*18*, *26*, *19*). We observed the same strong enrichment of microglia for crosstalk interactions involving AD genes in all three studies (**Supp. Figure 5**). We observed differences across studies regarding which neuronal cell type was most enriched for crosstalk interactions with microglia involving AD genes. Nonetheless, the enrichment direction of effect for excitatory neurons agreed with our findings in all studies. These results suggest that a

subset of genes previously implicated in AD mediate cell signaling pathways between neurons and microglia.

To further validate if the previous results were not driven by an overrepresentation bias of microglia interactions in the CellPhoneDB database, we used the control donors to calculate the enrichment of crosstalk interactions in genes found by GWAS for other neurological traits (**Supp. Table 5**). If the crosstalk interactions were biased towards one or a subset of cell types due to database overrepresentation, our expectation would be that we would observe similar enrichment patterns across traits. On the contrary, we observed distinct crosstalk enrichment patterns across neurological traits (**Figure 1g**). Crosstalk interactions involving oligodendrocyte precursors were significantly enriched for genes from one schizophrenia GWAS (OR = 2.64, adj. p = 3.12e-5). We also observed nominally significant enrichment for astrocyte crosstalk interactions for genes from a Parkinson's disease GWAS (OR = 2.45, p = 0.029). Importantly, we replicated the enrichment for microglia crosstalk interactions in genes from two independent AD GWAS (ORs = 3.39 and 3.07, adj. p = 3.16e-4 and 0.0023). We next used a strategy to nominate AD genes based on snATAC-seq co-accessibility between the gene promoter regions with a fine-mapped (*14*) AD GWAS variant (see Methods). This rigorous approach nominates candidate AD genes and their corresponding cell types based on direct evidence from functional genomics. We observed an even higher enrichment for microglia crosstalk interactions in AD (OR = 9.07, p = 1.24e-15; **Figure 1h**). In combination, these results indicate that the observed crosstalk enrichment patterns were not artificially biased toward any cell type. Furthermore, these analyses highlight that our crosstalk framework can be used to understand biological processes associated with GWAS variants for multiple neurological diseases.

Crosstalk interactions between microglia and excitatory neurons are predicted to modulate genes implicated in AD

We next sought to investigate how the crosstalk signals between neurons and microglia modulate downstream microglia gene regulatory networks. Using a system biology approach based on extending the functionality of the CytoTalk software (*27*) (see methods), we inferred the gene co-expression networks upstream of the ligands and downstream of the receptors. CytoTalk is complementary to CellPhoneDB, which does not inform the biological processes likely downstream of crosstalk interactions. Using CytoTalk, we reconstructed the gene regulatory network associated with crosstalk interactions between excitatory neurons and microglia (**Figure 2a-b**). Strikingly, the microglia co-expression network downstream of the neuron-microglia crosstalk interactions was enriched for genes previously associated with AD (cases OR range = 1.99 to 3.52, median = 3.06, adj. p range = 0.017 to 2.86e-8, median = 1.06e-4; **Figure 2c**). In addition, the microglia crosstalk network identified by CytoTalk was overall enriched for immune processes, including phagocytosis and cytokine production, among others (**Figure 2d**), consistent with neuron-microglia crosstalk interactions modulating microglia activation states (*28*). These results indicate that neuron-microglia crosstalk interactions propagate signals that modulate genes previously implicated in AD, including those involved in regulating microglial activation.

The SEMA6D-TREM2 crosstalk axis is predicted to modulate microglia activation and to be disrupted in late-stage AD

Among the seven crosstalk interactions prioritized by CytoTalk based on the co-expression network topology, we identified the crosstalk interaction between neuronal ligand semaphorin 6D (SEMA6D) and TREM2/TYROBP (**Figure 2b**). In the brain, semaphorin signaling was initially described as a mediator of axon guidance via the plexin family of receptors (*29*). However, an increasing body of evidence indicates that these molecules are also involved in immune responses. Notably, a study in bone marrow-derived macrophages discovered that the SEMA6D-PLXNA1 interaction induces macrophage activation in a TREM2-dependent manner via activation of DAP12 (*7*). Importantly, this study found that TREM2, PLXNA1, and DAP12 co-immunoprecipitate in a TREM2-dependent manner, consistent with the formation of a complex (*30*, *31*). Furthermore, additional studies also linked plexin-semaphorin signaling to immune activation and neurodegeneration (*5*, *22–24*, *32*). Given this role for SEMA6D in the immune activation of myeloid cells, we aimed to test the potential role of the SEMA6D-TREM2/PLXNA1 signaling axis in AD.

Using a clustering algorithm to divide the microglia crosstalk network into sub-networks (see methods), we identified a microglia sub-network comprised of a large clique of genes highly connected to *TREM2* and *TYROBP*. This TREM2 sub-network was predicted to be modulated by neuronal SEMA6D (**Figure 2e**). Furthermore, the TREM2 sub-network was enriched for microglia activation genes, indicating that we recapitulated the well-established link between TREM2 and microglia activation (*33*) through an unsupervised approach (**Figure 2d**). Interestingly, in addition to genes linked to microglia activation, the TREM2 crosstalk sub-network included *APOE* and *HLA* genes previously reported as AD risk genes. The connection between *TREM2* and *APOE* is consistent with studies showing that APOE is a TREM2 ligand (*34*, *35*) and suggests that the PLXNA1-SEMA6D crosstalk interaction modulates AD risk genes.

To validate these results, we repeated the CytoTalk analyses in the snRNA-seq studies from the SWDBB, Rush ADRC, and UCI MIND ADRC cohorts (*18*, *19*, *26*). Consistent with our original results, CytoTalk prioritized the SEMA6D-TREM2 signaling axis mediating the crosstalk interactions between exc. neurons and microglia in all three cohorts (**Supp. Figure 6a**). Finally, we determined that the TREM2 sub-network and its predicted modulation by SEMA6D were robust to the choice of donors and number of nuclei (**Supp. Figure 6b**). Together, these results reinforce that the unsupervised methodological approach in this study identified core elements of microglia gene regulation, which are predicted to be modulated by neuron-microglia cellular crosstalk interactions and are robust to brain donor and region.

We next sought to understand how the TREM2 sub-network related to AD progression. We leveraged the range of neuropathological states in our dataset to develop a statistical framework to test the association of this sub-network with the Braak stages, controlling for genetic and other confounding factors (see methods). Using this approach, we determined that the expression of the TREM2 sub-network was negatively associated with the Braak stages (beta = -0.31, adj. p = 4.32e-57). To contextualize this result, we calculated the association of all neuron-microglia crosstalk sub-networks with the Braak stages. Strikingly, the majority (11 of 14) of the microglia crosstalk sub-networks were negatively associated with the Braak stages, and the TREM2 sub-network was among the most negatively associated with Braak stages (**Figure 2f**). These results suggest that neuron-microglia crosstalk interactions and their

downstream targets in microglia are impaired in the later stages of AD. Next, we sought to determine if SEMA6D is a potential modulator of the TREM2 microglia crosstalk sub-network. We reasoned that if this were the case, the neuronal SEMA6D crosstalk sub-network direction of association with the Braak stages would agree with the TREM2 sub-network. Indeed, the neuronal SEMA6D sub-network was negatively associated with the Braak stages (beta = -0.09, adj. p = 1.63e-04; **Figure 2h**). Therefore, our findings indicate that the biological processes associated with the SEMA6D-PLXNA1 neuron-microglia crosstalk interactions are disrupted in AD and likely confer AD resilience by modulating TREM2-dependent microglia activation.

Multiple microglia co-expression sub-networks are disrupted during AD progression

We next adapted our network analysis framework to analyze the microglia co-expression network aiming to gain insights into the role of microglia in AD. This expanded approach allowed us to test the association of sub-networks not predicted to be directly involved in neuron-microglia crosstalk with the Braak stages (see methods). Using the entire reconstructed microglia co-expression network, we identified 360 sub-networks and recapitulated several crosstalk sub-networks identified previously with CytoTalk, including the TREM2 sub-network (**Supp. Figure 7**). These microglia sub-networks were divided between positive and negative associations with the Braak stages (**Figure 2g**). Consistent with the well-established roles of *PSEN1* and *APP* in AD onset (*36*), the *PSEN1* and *APP* co-expression sub-networks were among the most positively correlated with the Braak stages (betas = 0.32 and 0.16, adj. p = 8.25e-57 and 2.17e-13, respectively). In contrast, the sub-network of *SORL1*, a gene associated with protective roles in AD (*37*, *38*), was negatively associated with the Braak stages (beta = -0.15, adj. p = 3.52e-11). Interestingly, our unsupervised approach identified two separate sub-networks with opposing directions of effect for the genes in the MS4A locus, which genetically controls soluble TREM2 levels (*39*) (*MS4A4A* and *MS4A6A* betas = -0.11 and 0.19, adj. p = 2.87e-06 and 2.93e-20, respectively). This result suggests that the MS4A genetic signal regulates at least two independent biological processes, as we reported previously (*39*). Within the context of all microglia genes, the TREM2 sub-network was among the most negatively associated with the Braak stages, consistent with our previous analysis using the prioritized crosstalk network from CytoTalk. These results indicate that multiple biological pathways downstream of microglia-neuronal crosstalk are disrupted in AD. Furthermore, our unsupervised computational framework identifies impaired TREM2-dependent microglia activation as a contributing factor to AD progression.

SEMA6D treatment potentiates immune activation in iPSC-derived microglia in a TREM2-dependent manner

Microglia, among other functions, regulate brain homeostasis through phagocytic activity and modulate neuroinflammation by releasing inflammatory cytokines, such as TNF-α and IL-6 (*40*). We generated iMGL to examine if SEMA6D modulates iMGL functions (**Supp. Figure 8a**, see methods). (*41*) iMGL exhibited established microglia markers, including TREM2, IBA1, and TMEM119 (**Supp. Figure 8b**). We also generated *TREM2* knockout (KO) human iPSCs using CRISPR/Cas9 to examine the role of the SEMA6D-TREM2 signaling axis on microglia function (**Supp. Figure 8c**). We verified the loss of TREM2 expression at the protein level in the KO cell line by Western blot analysis (**Supp. Figure 8d**).

To determine if SEMA6D can regulate iMGL phagocytic activity and if this is TREM2 dependent, we treated WT and KO iMGL with SEMA6D protein and measured the degree of phagocytic activity on pHrodo-labeled human synaptosomes (**Supp. Figure 9**). Live-cell imaging over 24 hours showed increased phagocytosis of WT iMGL treated with SEMA6D starting after 6 hours. TREM2 KO iMGL treated with SEMA6D did not demonstrate increased phagocytosis compared to untreated TREM2 KO cells (**Figure 3a-b**). These results indicate that SEMA6D can modulate iMGL phagocytosis in a TREM2-dependent manner. We analyzed conditioned media using a multiplex immunoassay to determine if SEMA6D can regulate iMGL cytokine release mediated by TREM2from control or SEMA6D-treated iMGL. We found that SEMA6D increased the secretion of TNF-α and IL-6 in WT iMGL. SEMA6D did not increase cytokine release in TREM2 KO iMGL (**Figure 3c**). SEMA6D regulation of iMGL cytokine release also appears to be TREM2 dependent.

TREM2 mediates signaling through the adaptor protein TYROBP (DAP12). Activation of TREM2 results in tyrosine phosphorylation within the ITAM motif and subsequent SYK phosphorylation (**Figure 3f**) (*42*). To determine if SEMA6D activates TREM2 downstream signaling, we analyzed WT and KO iMGL lysates for phosphorylated SYK expression (p-SYK) normalized to total SYK expression (SYK). Treatment of WT iMGL with SEMA6D induced SYK phosphorylation, while KO iMGL did not. (**Figure 3d**)**-e**.). This demonstrates that SEMA6D can activate TREM2 signaling and suggests that SEMA6D signals through the PLXNA1/TREM2/DAP12 complex.

In parallel, to understand the regulatory changes induced by SEMA6D treatment in iMGL, we generated bulk RNA-seq data for the SEMA6D-treated and control WT and KO iMGL (**Supp. Figure 10**). We observed significant changes in gene expression associated with TREM2 KO (**Supp. Figure 10a-b**). As expected, *TREM2* was among the most downregulated genes in the KO iMGL (**Supp. Figure 10a**). Strikingly, we observed robust transcriptional changes in WT SEMA6D-treated iMGL but not *TREM2* KO iMGL (**Figure 3g; Supp. Figure 10a-b**), supporting a pivotal role for TREM2 in mediating SEMA6D-PLXNA1 crosstalk signaling. To further understand how TREM2 modulates this crosstalk, we focused on the *TREM2* co-expression sub-network we predicted from the snRNA-seq data using CytoTalk. The *TREM2* sub-network had significantly lower expression in the untreated KO iMGL compared to WT, consistent with TREM2 being a key regulator of this sub-network. In line with this interpretation, the TREM2 sub-network was activated by SEMA6D treatment in the WT iMGL but significantly less so in the KO iMGL (**Figure 3h-i**).

To gain further insights into how SEMA6D treatment regulates microglial transcriptional programs, we checked biologically relevant transcriptional signatures previously described in microglia. These included genes up-regulated in phagocytosing microglia (*43*) and those up-regulated in response to LPS treatment (*20*). As control signatures, we included genes down-regulated in TREM2 KO iMGL (*44*) and a set of randomly selected genes for which we would not expect any concerted transcriptional changes. We observed the strongest effects (Log2FC >0.4) of SEMA6D treatment in the phagocytosing microglia gene signature (**Figure 3i**), indicating that SEMA6D activates genes crucial to phagocytosis in the WT but not TREM2 KO iMGL. Notably, TREM2, APOE, and RPS19 are among the most up-regulated genes by SEMA6D treatment in the WT iMGL, which were either present in the phagocytosing microglia gene signature or correspond to genes previously linked to microglia activation (*45*, *17*) (**Figure**

3j). Our results indicate that SEMA6D-TREM2 crosstalk signaling induces a TREM2-mediated cascade of transcriptional events resulting in microglia activation.

Discussion

In this study, we leveraged single-nucleus gene expression profiles from a diverse cohort of brain donors to systematically dissect the contribution of cross-cellular signaling (cellular crosstalk) networks to AD progression. Our data-driven approach to identifying active crosstalk interactions and reconstructing their corresponding downstream pathways provides additional evidence that disrupted cellular crosstalk networks contribute to neurodegeneration. One remarkable finding from our study is that a significant portion of AD risk genes are either directly involved in crosstalk interactions or immediately downstream of microglia interactions. These results highlight the difficulty of characterizing the prominent role of microglia in AD progression, as these cells integrate complex signals originating in other brain cell types. Specifically, our results support that dysregulation in the intricate signaling between neurons and microglia is linked to AD progression. Therefore, focusing on cellular crosstalk networks can provide further functional context to understand the biology of genes associated with AD risk in a cell non-autonomous and autonomous manner.

Among the interactions we detected between neurons and microglia, we identified a novel functional link between neuronal SEMA6D and microglial TREM2. Furthermore, by leveraging iMGL, we demonstrate that SEMA6D signaling induces a TREM2-dependent microglia activation phenotype transcriptionally similar to phagocytosing microglia (*43*). These results, combined with our observation that the transcriptional networks upstream and downstream of the SEMA6D-PLXNA1 interaction are downregulated in AD, suggest that loss of this crosstalk interaction exacerbates the deleterious processes occurring in the later stages of this disease.

We used iMGL to demonstrate that SEMA6D promotes microglial phagocytosis and inflammatory cytokine release. SEMA6D-induced microglial and downstream SYK activation were not observed in the TREM2 KO iMGL. Previous reports showed that SEMA6D promotes peripheral dendritic cell activation and osteoclast differentiation via the receptor complex harboring PLXNA1 and TREM2 (*46*). Thus, it is conceivable that SEMA6D functions as a natural ligand for the PLXNA1/TREM2 co-receptor and enhances TREM2 signaling in human microglia. Therefore, neuronal SEMA6D could influence functional properties and fate via the stimulation of TREM2-dependent intracellular signaling and induction of TREM2-network gene expression. Nevertheless, it remains to be determined if SEMA6D induces an anti-inflammatory state of microglia that might be beneficial in clearing neuropathological changes associated with AD.

SEMA6D also regulates lipid metabolism and polarization of macrophages via the interaction with another class A plexin family member, PlexinA4 (*47*, *48*). Several coding variants in PlexinA4 are associated with AD risk (*48*, *49*) and modulate both amyloid and tau pathology (*50*). Thus, semaphorin-plexin signaling may play a fundamental role in regulating the functional interactions between glutaminergic neurons and a subset of microglia and may be perturbed in AD.

While this study focused on a restricted subset of crosstalk interactions involving microglia and neurons, our systematic characterization of cross-cellular signaling patterns identified thousands

of candidate interactions involving all brain cell types represented in our snRNA-seq data. Some of these interactions warrant further investigation. For example, the interleukin receptor IL1RAP has been previously implicated in genetic studies of AD endophenotypes (*3*, *51–53*), and the contribution of IL-1 signaling to neurodegenerative diseases has been well-established (*54–56*). In line with these previous findings, we identified the *IL1RAP* sub-network in microglia as the most negatively associated with the Braak stages. These results suggest that disruption of the IL-1 signaling pathway is likely to be involved in AD progression. More broadly, the IL1RAP case highlights that the continued exploration of brain crosstalk networks identified in this study will yield valuable biological insights into AD biology. Finally, we identified distinct crosstalk enrichment patterns for genes identified by genetic studies of other neurological traits or diseases. These results emphasize that cellular crosstalk is an integral part of normal brain physiology, and accounting for this regulatory layer will help contextualize how candidate disease risk genes fit into biological pathways. Together, our findings offer a strong rationale that the systematic characterization of cellular crosstalk networks is a viable strategy for gaining insight into the biology of neurodegenerative diseases.

Acknowledgments

Data collection and sharing for this project was supported by The Dominantly Inherited Alzheimer Network (DIAN, U19AG032438), funded by the National Institute on Aging (NIA), the Alzheimer's Association (SG-20-690363-DIAN), the German Center for Neurodegenerative Diseases (DZNE), Raul Carrea Institute for Neurological Research (FLENI), Partial support by the Research and Development Grants for Dementia from Japan Agency for Medical Research and Development, AMED, and the Korea Health Technology R&D Project through the Korea Health Industry Development Institute (KHIDI), Spanish Institute of Health Carlos III (ISCIII), Canadian Institutes of Health Research (CIHR), Canadian Consortium of Neurodegeneration and Aging, Brain Canada Foundation, and Fonds de Recherche du Québec – Santé. This manuscript has been reviewed by DIAN Study investigatorsfor scientific content and consistency of data interpretation with previous DIAN Study publications. We acknowledge the altruism of the participants and their families and the contributions of the DIAN research and support staff at each of the participating sites for their contributions to this study. This research was supported by NIH grants R01 AG067606 (to T.-W.K), AG072464 (CMK, OH), NINDS R01NS118146 and R21NS127211 (to BAB), NIH AG062734 (CMK), and R56AG067764 (GS). Additional funding from the Chan Zuckerberg Initiative (CMK, OH, CC). We thank Barbara Corneo for advice on iPSC protocols, and Barbara Corneo, Wei Wang; Caisheng (Luke) Lu, MD, Ph.D. for assisting FACS sorting. IMGL sequencing and preliminary data processing was conducted by Novogene.

Author contributions

OOO

Competing interests

T.-W.K. is a cofounder of BL Melanis Co. Ltd.

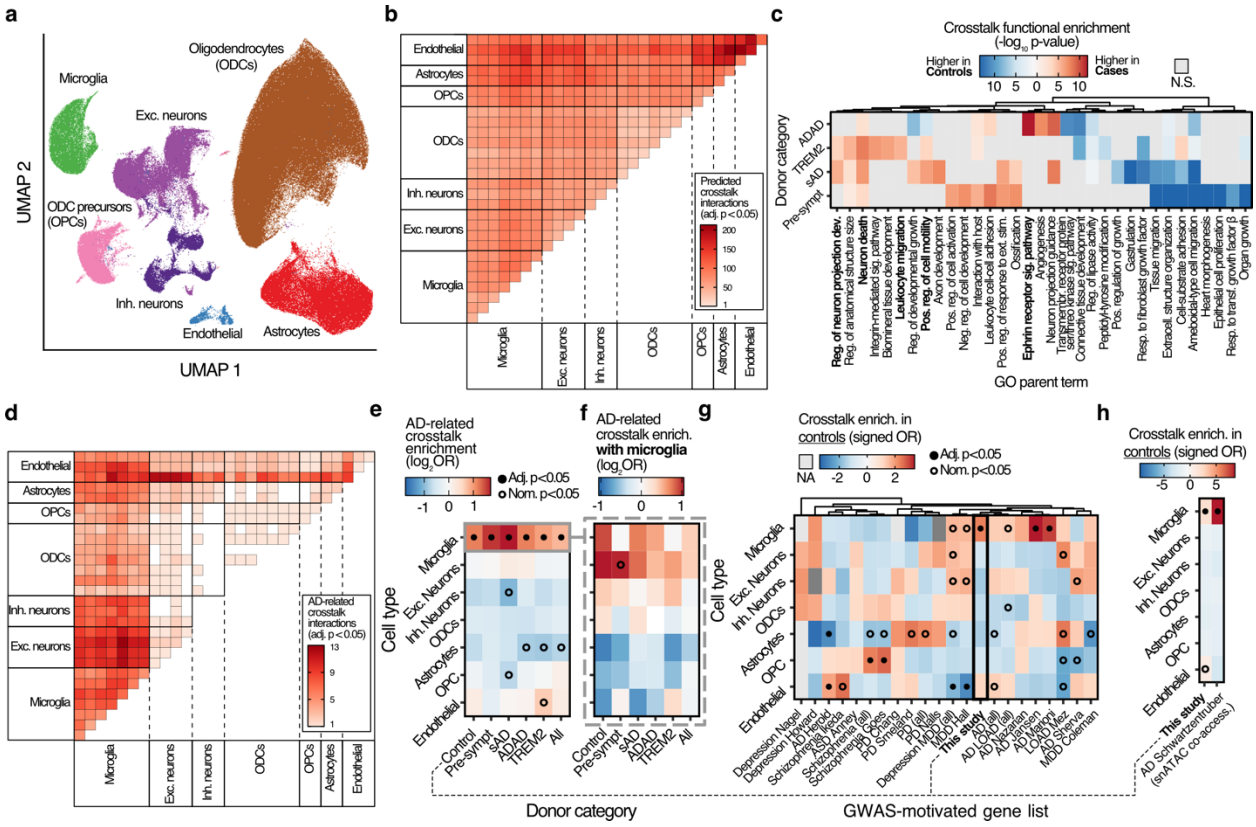

Figure 1: Overview of predicted cellular crosstalk patterns in human brains during health and AD. a) Uniform Manifold Approximation and Projection (UMAP) representation of the snRNA-seq dataset. **b)** Number of unique significant CellPhoneDB interactions detected involving each cell type as either the ligand or receptor across donor categories. **c)** Gene ontology enrichments of crosstalk interactions up- or down-regulated between each donor category versus controls. **d)** Cellular crosstalk interactions involving one AD gene as either ligand or receptor across all cellular state pairs. **e)** Enrichment of AD crosstalk interactions involving each cell type in each donor category. **f)** Enrichment of AD crosstalk interactions between microglia and other cell types (labeled in the y-axis). **g)** Crosstalk enrichments for each cell type (control donors only) in genes nominated by GWAS in other neuropsychiatric traits. **h)** Similar to (**g**) but using only AD genes supported by snATAC-seq co-accessibility (Methods). Odds ratios in (**e-h)** were calculated using Fisher exact tests (Methods).

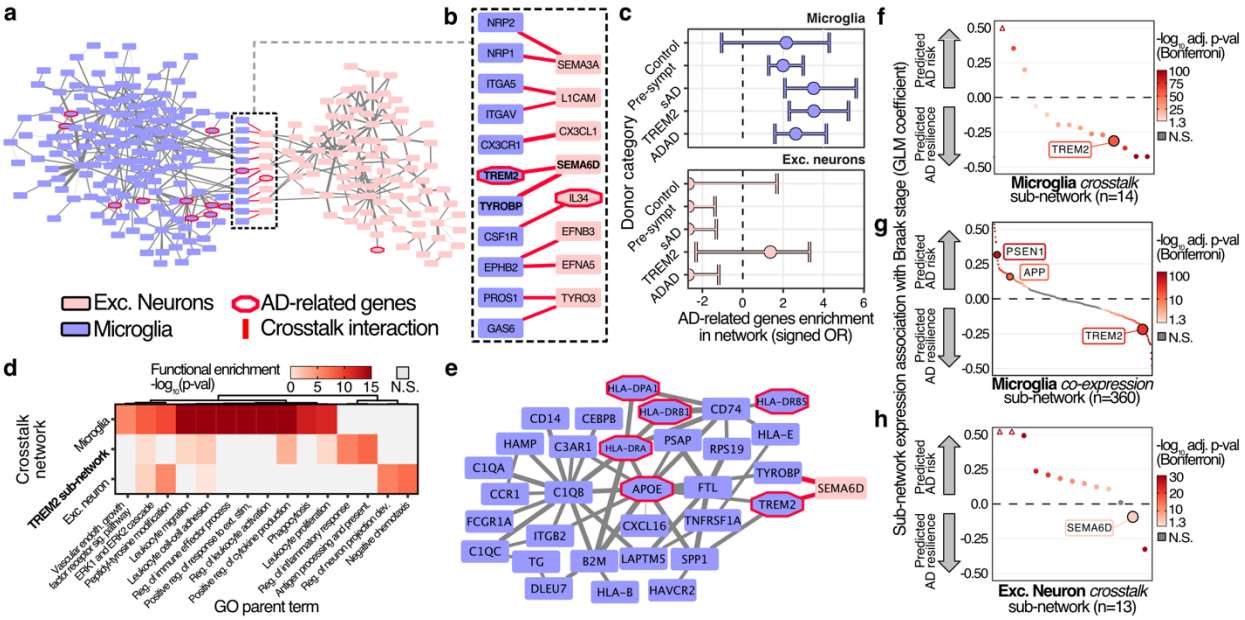

Figure 2: Crosstalk interactions between neurons and microglia are predicted to modulate AD risk genes. a) Microglia-excitatory neuron crosstalk network inferred by CytoTalk. **b)** Prioritized crosstalk interactions using CytoTalk. **c)** Enrichment of AD genes in the microglia crosstalk network across donor categories. **d**) GO enrichments for the genes participating in microglia and excitatory neurons crosstalk networks. **e)** Predicted TREM2 crosstalk subnetwork **f)** Association of microglia crosstalk subnetworks with Braak stages. **g)** Association of all microglia subnetworks with Braak stages. **h)** Association excitatory neuron crosstalk subnetworks with the Braak stages.

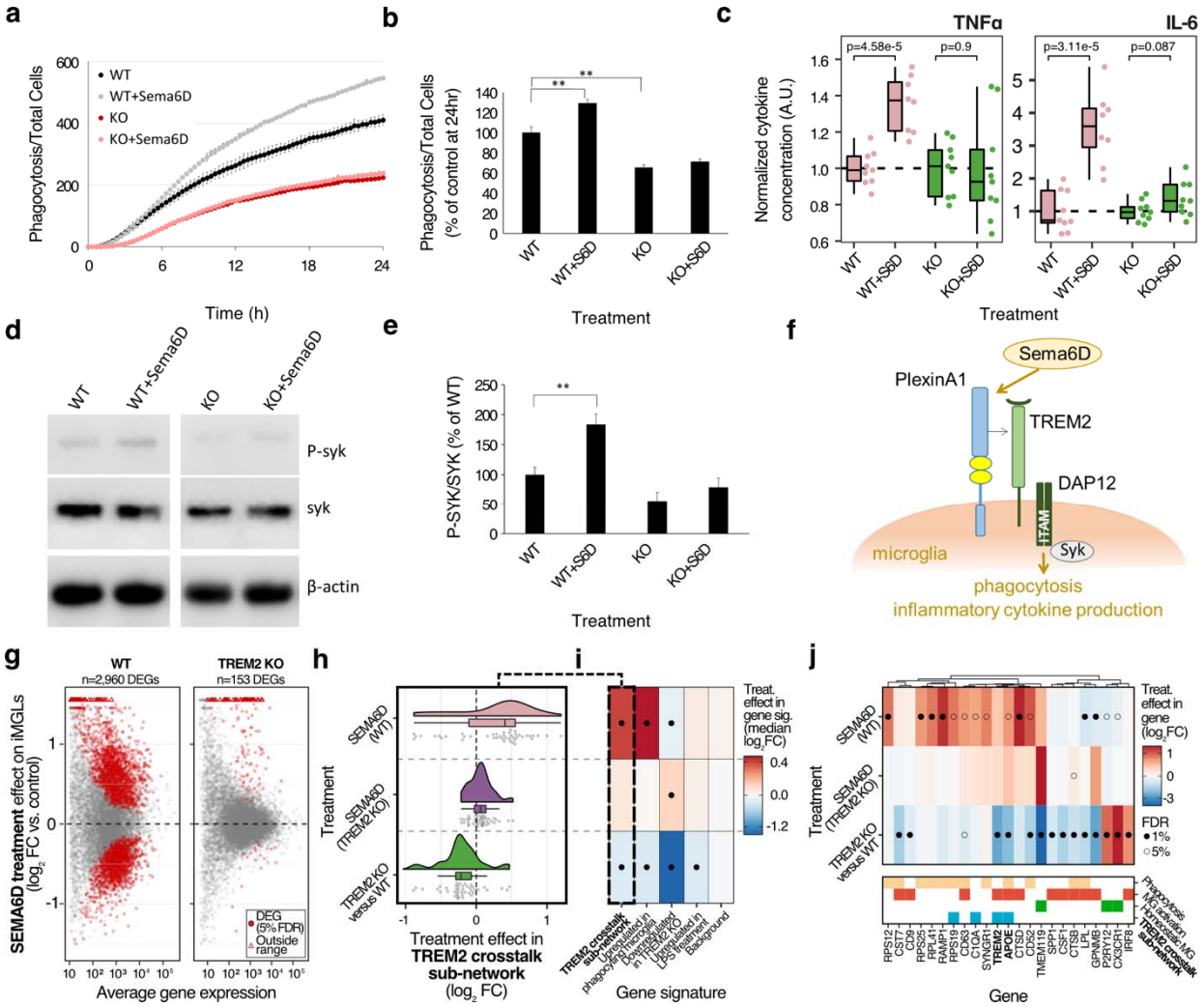

Figure 3. SEMA6D treatment induces microglia activation in a TREM2-dependent manner. **a)** Representative graph of phagocytosis of synaptosomes by WT or TREM2 KO iMGL treated with Sema6D (5 µg 5ug/ml). **b)** Quantification of phagocytosis of synaptosomes by WT or TREM2 KO iMGL treated with Sema6D at 24 hr. Data represent three independent experiments performed in triplicate; mean ± SEM unpaired two-tailed t-test, $^{**}p < 0.01$ at 24 hrs. **c)** Quantification of media from WT or KO iMGL treated with Sema6D (10 µg/ml) for cytokine release of TNF-α and IL-6, using the Mesoscale V-plex neuroinflammation panel. **d)** Representative western blot analysis of p-SYK and total SYK in WT and KO iMGL treated with Sema6D (10 µg/ml). β-actin as loading control **e)** Quantification of p-SYK/total SYK western blot analysis, n=3 **(d)**. **f)** Schematic of the proposed PlexinA-TREM2/DAP12 signaling complex. **g)** RNA-seq effect size distribution on SEMA6D-treated iMGL (WT and *TREM2* KO). **h)** Transcriptional changes associated with SEMA6D treatment (WT or *TREM2* KO vs. control) or TREM2 knockout (KO vs. WT, no treatment) in the TREM2 crosstalk sub-network. Only TREM2 sub-network genes differentially expressed in at least one comparison were included. **i)** Transcriptional effects of the same conditions as **(b)** across biologically relevant gene signatures. Background corresponds to 500 randomly selected genes. Dots correspond to a 1% FDR significance threshold for comparing the effect size distribution to the corresponding background in each comparison (Wilcoxon rank-sum test). **j)** Transcriptional effects of the conditions across highly differentially expressed genes from a subset of signatures in **(i)**.

References

1. D. P. Schafer, E. K. Lehrman, A. G. Kautzman, R. Koyama, A. R. Mardinly, R. Yamasaki, R. M. Ransohoff, M. E. Greenberg, B. A. Barres, B. Stevens, Microglia sculpt postnatal neural circuits in an activity and complement-dependent manner. *Neuron*. **74**, 691–705 (2012).

2. D. Fard, L. Tamagnone, Semaphorins in health and disease. *Cytokine Growth Factor Rev*. **57**, 55–63 (2021).

3. V. K. Ramanan, S. L. Risacher, K. Nho, S. Kim, L. Shen, B. C. McDonald, K. K. Yoder, G. D. Hutchins, J. D. West, E. F. Tallman, S. Gao, T. M. Foroud, M. R. Farlow, P. L. De Jager, D. A. Bennett, P. S. Aisen, R. C. Petersen, C. R. Jack, A. W. Toga, R. C. Green, W. J. Jagust, M. W. Weiner, A. J. Saykin, Alzheimer's Disease Neuroimaging Initiative (ADNI), GWAS of longitudinal amyloid accumulation on 18F-florbetapir PET in Alzheimer's disease implicates microglial activation gene IL1RAP. *Brain*. **138**, 3076–3088 (2015).

4. C. S. McAlpine, J. Park, A. Griciuc, E. Kim, S. H. Choi, Y. Iwamoto, M. G. Kiss, K. A. Christie, C. Vinegoni, W. C. Poller, J. E. Mindur, C. T. Chan, S. He, H. Janssen, L. P. Wong, J. Downey, S. Singh, A. Anzai, F. Kahles, M. Jorfi, P. F. Feruglio, R. I. Sadreyev, R. Weissleder, B. P. Kleinstiver, M. Nahrendorf, R. E. Tanzi, F. K. Swirski, Astrocytic interleukin-3 programs microglia and limits Alzheimer's disease. *Nature* (2021), doi:10.1038/s41586-021-03734-6.

5. I. C. Clark, C. Gutiérrez-Vázquez, M. A. Wheeler, Z. Li, V. Rothhammer, M. Linnerbauer, L. M. Sanmarco, L. Guo, M. Blain, S. E. J. Zandee, C.-C. Chao, K. V. Batterman, M. Schwabenland, P. Lotfy, A. Tejeda-Velarde, P. Hewson, C. Manganeli Polonio, M. W. Shultis, Y. Salem, E. C. Tjon, P. H. Fonseca-Castro, D. M. Borucki, K. Alves de Lima, A. Plasencia, A. R. Abate, D. L. Rosene, K. J. Hodgetts, M. Prinz, J. P. Antel, A. Prat, F. J. Quintana, Barcoded viral tracing of single-cell interactions in central nervous system inflammation. *Science*. **372**, eabf1230 (2021).

6. H. Lian, A. Litvinchuk, A. C.-A. Chiang, N. Aithmitti, J. L. Jankowsky, H. Zheng, Astrocyte-Microglia Cross Talk through Complement Activation Modulates Amyloid Pathology in Mouse Models of Alzheimer's Disease. *J Neurosci*. **36**, 577–589 (2016).

7. N. Takegahara, H. Takamatsu, T. Toyofuku, T. Tsujimura, T. Okuno, K. Yukawa, M. Mizui, M. Yamamoto, D. V. R. Prasad, K. Suzuki, M. Ishii, K. Terai, M. Moriya, Y. Nakatsuji, S. Sakoda, S. Sato, S. Akira, K. Takeda, M. Inui, T. Takai, M. Ikawa, M. Okabe, A. Kumanogoh, H. Kikutani, Plexin-A1 and its interaction with DAP12 in immune responses and bone homeostasis. *Nat Cell Biol*. **8**, 615–622 (2006).

8. T. Ito, K. Yoshida, T. Negishi, M. Miyajima, H. Takamatsu, H. Kikutani, A. Kumanogoh, K. Yukawa, Plexin-A1 is required for Toll-like receptor-mediated microglial activation in the development of lipopolysaccharide-induced encephalopathy. *Int J Mol Med*. **33**, 1122–1130 (2014).

9. H. Yin, A. D. Flynn, Drugging Membrane Protein Interactions. *Annu Rev Biomed Eng*. **18**, 51–76 (2016).

10. J. P. Overington, B. Al-Lazikani, A. L. Hopkins, How many drug targets are there? *Nat Rev Drug Discov*. **5**, 993–996 (2006).

11. T. Worzfeld, S. Offermanns, Semaphorins and plexins as therapeutic targets. *Nat Rev Drug Discov*. **13**, 603–621 (2014).

12. J. C. Lambert, C. A. Ibrahim-Verbaas, D. Harold, A. C. Naj, R. Sims, C. Bellenguez, A. L. DeStafano, J. C. Bis, G. W. Beecham, B. Grenier-Boley, G. Russo, T. A. Thorton-Wells, N. Jones, A. V. Smith, V. Chouraki, C. Thomas, M. A. Ikram, D. Zelenika, B. N. Vardarajan, Y. Kamatani, C. F. Lin, A. Gerrish, H. Schmidt, B. Kunkle, M. L. Dunstan, A. Ruiz, M. T. Bihoreau, S. H. Choi, C. Reitz, F. Pasquier, C. Cruchaga, D. Craig, N. Amin, C. Berr, O. L. Lopez, P. L. De Jager, V. Deramecourt, J. A. Johnston, D. Evans, S. Lovestone, L. Letenneur, F. J. Morón, D. C. Rubinsztein, G. Eiriksdottir, K. Sleegers, A. M. Goate, N. Fiévet, M. W. Huentelman, M. Gill, K. Brown, M. I. Kamboh, L. Keller, P. Barberger-Gateau, B. McGuiness, E. B. Larson, R. Green, A. J. Myers, C. Dufouil, S. Todd, D. Wallon, S. Love, E. Rogaeva, J. Gallacher, P. St George-Hyslop, J. Clarimon, A. Lleo, A. Bayer, D. W. Tsuang, L. Yu, M. Tsolaki, P. Bossù, G. Spalletta, P. Proitsi, J. Collinge, S. Sorbi, F. Sanchez-Garcia, N. C. Fox, J. Hardy, M. C. Deniz Naranjo, P. Bosco, R. Clarke, C. Brayne, D. Galimberti, M. Mancuso, F. Matthews, European Alzheimer's Disease Initiative (EADI), Genetic and Environmental Risk in Alzheimer's Disease, Alzheimer's Disease Genetic Consortium, Cohorts for Heart and Aging Research in Genomic Epidemiology, S. Moebus, P. Mecocci, M. Del Zompo, W. Maier, H. Hampel, A. Pilotto, M. Bullido, F. Panza, P. Caffarra, B. Nacmias, J. R. Gilbert, M. Mayhaus, L. Lannefelt, H. Hakonarson, S. Pichler, M. M. Carrasquillo, M. Ingelsson, D. Beekly, V. Alvarez, F. Zou, O. Valladares, S. G. Younkin, E. Coto, K. L. Hamilton-Nelson, W. Gu, C. Razquin, P. Pastor, I. Mateo, M. J. Owen, K. M. Faber, P. V. Jonsson, O. Combarros, M. C. O'Donovan, L. B. Cantwell, H. Soininen, D. Blacker, S. Mead, T. H. Mosley, D. A. Bennett, T. B. Harris, L. Fratiglioni, C. Holmes, R. F. de Bruijn, P. Passmore, T. J. Montine, K. Bettens, J. I. Rotter, A. Brice, K. Morgan, T. M. Foroud, W. A. Kukull, D. Hannequin, J. F. Powell, M. A. Nalls, K. Ritchie, K. L. Lunetta, J. S. Kauwe, E. Boerwinkle, M. Riemenschneider, M. Boada, M. Hiltuenen, E. R. Martin, R. Schmidt, D. Rujescu, L. S. Wang, J. F. Dartigues, R. Mayeux, C. Tzourio, A. Hofman, M. M. Nöthen, C. Graff, B. M. Psaty, L. Jones, J. L. Haines, P. A. Holmans, M. Lathrop, M. A. Pericak-Vance, L. J. Launer, L. A. Farrer, C. M. van Duijn, C. Van Broeckhoven, V. Moskvina, S. Seshadri, J. Williams, G. D. Schellenberg, P. Amouyel, Meta-analysis of 74,046 individuals identifies 11 new susceptibility loci for Alzheimer's disease. *Nat Genet*. **45**, 1452–1458 (2013).

13. B. W. Kunkle, B. Grenier-Boley, R. Sims, J. C. Bis, V. Damotte, A. C. Naj, A. Boland, M. Vronskaya, S. J. van der Lee, A. Amlie-Wolf, C. Bellenguez, A. Frizatti, V. Chouraki, E. R. Martin, K. Sleegers, N. Badarinarayan, J. Jakobsdottir, K. L. Hamilton-Nelson, S. Moreno-Grau, R. Olaso, R. Raybould, Y. Chen, A. B. Kuzma, M. Hiltunen, T. Morgan, S. Ahmad, B. N. Vardarajan, J. Epelbaum, P. Hoffmann, M. Boada, G. W. Beecham, J.-G. Garnier, D. Harold, A. L. Fitzpatrick, O. Valladares, M.-L. Moutet, A. Gerrish, A. V. Smith, L. Qu, D. Bacq, N. Denning, X. Jian, Y. Zhao, M. Del Zompo, N. C. Fox, S.-H. Choi, I. Mateo, J. T. Hughes, H. H. Adams, J. Malamon, F. Sanchez-Garcia, Y. Patel, J. A. Brody, B. A. Dombroski, M. C. D. Naranjo, M. Daniilidou, G. Eiriksdottir, S. Mukherjee, D. Wallon, J. Uphill, T. Aspelund, L. B. Cantwell, F. Garzia, D. Galimberti, E. Hofer, M. Butkiewicz, B. Fin, E. Scarpini, C. Sarnowski, W. S. Bush, S. Meslage, J. Kornhuber, C. C. White, Y. Song, R. C. Barber, S. Engelborghs, S. Sordon, D. Voijnovic, P. M. Adams, R. Vandenberghe, M. Mayhaus, L. A. Cupples, M. S. Albert, P. P. De Deyn, W. Gu, J. J. Himali, D. Beekly, A. Squassina, A. M. Hartmann, A. Orellana, D. Blacker, E. Rodriguez-

Rodriguez, S. Lovestone, M. E. Garcia, R. S. Doody, C. Munoz-Fernadez, R. Sussams, H. Lin, T. J. Fairchild, Y. A. Benito, C. Holmes, H. Karamujić-Čomić, M. P. Frosch, H. Thonberg, W. Maier, G. Roshchupkin, B. Ghetti, V. Giedraitis, A. Kawalia, S. Li, R. M. Huebinger, L. Kilander, S. Moebus, I. Hernández, M. I. Kamboh, R. Brundin, J. Turton, Q. Yang, M. J. Katz, L. Concari, J. Lord, A. S. Beiser, C. D. Keene, S. Helisalmi, I. Kloszewska, W. A. Kukull, A. M. Koivisto, A. Lynch, L. Tarraga, E. B. Larson, A. Haapasalo, B. Lawlor, T. H. Mosley, R. B. Lipton, V. Solfrizzi, M. Gill, W. T. Longstreth, T. J. Montine, V. Frisardi, M. Diez-Fairen, F. Rivadeneira, R. C. Petersen, V. Deramecourt, I. Alvarez, F. Salani, A. Ciaramella, E. Boerwinkle, E. M. Reiman, N. Fievet, J. I. Rotter, J. S. Reisch, O. Hanon, C. Cupidi, A. G. Andre Uitterlinden, D. R. Royall, C. Dufouil, R. G. Maletta, I. de Rojas, M. Sano, A. Brice, R. Cecchetti, P. S. George-Hyslop, K. Ritchie, M. Tsolaki, D. W. Tsuang, B. Dubois, D. Craig, C.-K. Wu, H. Soininen, D. Avramidou, R. L. Albin, L. Fratiglioni, A. Germanou, L. G. Apostolova, L. Keller, M. Koutroumani, S. E. Arnold, F. Panza, O. Gkatzima, S. Asthana, D. Hannequin, P. Whitehead, C. S. Atwood, P. Caffarra, H. Hampel, I. Quintela, Á. Carracedo, L. Lannfelt, D. C. Rubinsztein, L. L. Barnes, F. Pasquier, L. Frölich, S. Barral, B. McGuinness, T. G. Beach, J. A. Johnston, J. T. Becker, P. Passmore, E. H. Bigio, J. M. Schott, T. D. Bird, J. D. Warren, B. F. Boeve, M. K. Lupton, J. D. Bowen, P. Proitsi, A. Boxer, J. F. Powell, J. R. Burke, J. S. K. Kauwe, J. M. Burns, M. Mancuso, J. D. Buxbaum, U. Bonuccelli, N. J. Cairns, A. McQuillin, C. Cao, G. Livingston, C. S. Carlson, N. J. Bass, C. M. Carlsson, J. Hardy, R. M. Carney, J. Bras, M. M. Carrasquillo, R. Guerreiro, M. Allen, H. C. Chui, E. Fisher, C. Masullo, E. A. Crocco, C. DeCarli, G. Bisceglio, M. Dick, L. Ma, R. Duara, N. R. Graff-Radford, D. A. Evans, A. Hodges, K. M. Faber, M. Scherer, K. B. Fallon, M. Riemenschneider, D. W. Fardo, R. Heun, M. R. Farlow, H. Kölsch, S. Ferris, M. Leber, T. M. Foroud, I. Heuser, D. R. Galasko, I. Giegling, M. Gearing, M. Hüll, D. H. Geschwind, J. R. Gilbert, J. Morris, R. C. Green, K. Mayo, J. H. Growdon, T. Feulner, R. L. Hamilton, L. E. Harrell, D. Drichel, L. S. Honig, T. D. Cushion, M. J. Huentelman, P. Hollingworth, C. M. Hulette, B. T. Hyman, R. Marshall, G. P. Jarvik, A. Meggy, E. Abner, G. E. Menzies, L.-W. Jin, G. Leonenko, L. M. Real, G. R. Jun, C. T. Baldwin, D. Grozeva, A. Karydas, G. Russo, J. A. Kaye, R. Kim, F. Jessen, N. W. Kowall, B. Vellas, J. H. Kramer, E. Vardy, F. M. LaFerla, K.-H. Jöckel, J. J. Lah, M. Dichgans, J. B. Leverenz, D. Mann, A. I. Levey, S. Pickering-Brown, A. P. Lieberman, N. Klopp, K. L. Lunetta, H.-E. Wichmann, C. G. Lyketsos, K. Morgan, D. C. Marson, K. Brown, F. Martiniuk, C. Medway, D. C. Mash, M. M. Nöthen, E. Masliah, N. M. Hooper, W. C. McCormick, A. Daniele, S. M. McCurry, A. Bayer, A. N. McDavid, J. Gallacher, A. C. McKee, H. van den Bussche, M. Mesulam, C. Brayne, B. L. Miller, S. Riedel-Heller, C. A. Miller, J. W. Miller, A. Al-Chalabi, J. C. Morris, C. E. Shaw, A. J. Myers, J. Wiltfang, S. O'Bryant, J. M. Olichney, V. Alvarez, J. E. Parisi, A. B. Singleton, H. L. Paulson, J. Collinge, W. R. Perry, S. Mead, E. Peskind, D. H. Cribbs, M. Rossor, A. Pierce, N. S. Ryan, W. W. Poon, B. Nacmias, H. Potter, S. Sorbi, J. F. Quinn, E. Sacchinelli, A. Raj, G. Spalletta, M. Raskind, C. Caltagirone, P. Bossù, M. D. Orfei, B. Reisberg, R. Clarke, C. Reitz, A. D. Smith, J. M. Ringman, D. Warden, E. D. Roberson, G. Wilcock, E. Rogaeva, A. C. Bruni, H. J. Rosen, M. Gallo, R. N. Rosenberg, Y. Ben-Shlomo, M. A. Sager, P. Mecocci, A. J. Saykin, P. Pastor, M. L. Cuccaro, J. M. Vance, J. A. Schneider, L. S. Schneider, S. Slifer, W. W. Seeley, A. G. Smith, J. A. Sonnen, S. Spina, R. A. Stern, R. H. Swerdlow, M. Tang, R. E. Tanzi, J. Q. Trojanowski, J. C. Troncoso, V. M. Van Deerlin, L. J. Van Eldik, H. V. Vinters, J. P. Vonsattel, S. Weintraub, K. A. Welsh-Bohmer, K. C. Wilhelmsen, J. Williamson, T. S. Wingo, R. L. Woltjer, C. B. Wright, C.-E. Yu, L. Yu, Y. Saba, A. Pilotto, M. J. Bullido, O. Peters, P. K. Crane, D. Bennett, P. Bosco, E. Coto, V. Boccardi, P. L. De Jager, A. Lleo, N. Warner, O. L. Lopez, M. Ingelsson, P. Deloukas, C. Cruchaga, C. Graff, R. Gwilliam, M. Fornage, A. M. Goate, P. Sanchez-Juan, P. G. Kehoe, N. Amin, N. Ertekin-Taner, C. Berr, S. Debette, S. Love, L. J. Launer, S. G. Younkin, J.-F.

Dartigues, C. Corcoran, M. A. Ikram, D. W. Dickson, G. Nicolas, D. Campion, J. Tschanz, H. Schmidt, H. Hakonarson, J. Clarimon, R. Munger, R. Schmidt, L. A. Farrer, C. Van Broeckhoven, M. C. O'Donovan, A. L. DeStefano, L. Jones, J. L. Haines, J.-F. Deleuze, M. J. Owen, V. Gudnason, R. Mayeux, V. Escott-Price, B. M. Psaty, A. Ramirez, L.-S. Wang, A. Ruiz, C. M. van Duijn, P. A. Holmans, S. Seshadri, J. Williams, P. Amouyel, G. D. Schellenberg, J.-C. Lambert, M. A. Pericak-Vance, Genetic meta-analysis of diagnosed Alzheimer's disease identifies new risk loci and implicates Aβ, tau, immunity and lipid processing. *Nat Genet*. **51**, 414–430 (2019).

14. J. Schwartzentruber, S. Cooper, J. Z. Liu, I. Barrio-Hernandez, E. Bello, N. Kumasaka, A. M. H. Young, R. J. M. Franklin, T. Johnson, K. Estrada, D. J. Gaffney, P. Beltrao, A. Bassett, Genome-wide meta-analysis, fine-mapping and integrative prioritization implicate new Alzheimer's disease risk genes. *Nat Genet*. **53**, 392–402 (2021).

15. C. Bellenguez, F. Küçükali, I. E. Jansen, L. Kleineidam, S. Moreno-Grau, N. Amin, A. C. Naj, R. Campos-Martin, B. Grenier-Boley, V. Andrade, P. A. Holmans, A. Boland, V. Damotte, S. J. van der Lee, M. R. Costa, T. Kuulasmaa, Q. Yang, I. de Rojas, J. C. Bis, A. Yaqub, I. Prokic, J. Chapuis, S. Ahmad, V. Giedraitis, D. Aarsland, P. Garcia-Gonzalez, C. Abdelnour, E. Alarcón-Martín, D. Alcolea, M. Alegret, I. Alvarez, V. Álvarez, N. J. Armstrong, A. Tsolaki, C. Antúnez, I. Appollonio, M. Arcaro, S. Archetti, A. A. Pastor, B. Arosio, L. Athanasiu, H. Bailly, N. Banaj, M. Baquero, S. Barral, A. Beiser, A. B. Pastor, J. E. Below, P. Benchek, L. Benussi, C. Berr, C. Besse, V. Bessi, G. Binetti, A. Bizarro, R. Blesa, M. Boada, E. Boerwinkle, B. Borroni, S. Boschi, P. Bossù, G. Bråthen, J. Bressler, C. Bresner, H. Brodaty, K. J. Brookes, L. I. Brusco, D. Buiza-Rueda, K. Bûrger, V. Burholt, W. S. Bush, M. Calero, L. B. Cantwell, G. Chene, J. Chung, M. L. Cuccaro, Á. Carracedo, R. Cecchetti, L. Cervera-Carles, C. Charbonnier, H.-H. Chen, C. Chillotti, S. Ciccone, J. A. H. R. Claassen, C. Clark, E. Conti, A. Corma-Gómez, E. Costantini, C. Custodero, D. Daian, M. C. Dalmasso, A. Daniele, E. Dardiotis, J.-F. Dartigues, P. P. de Deyn, K. de Paiva Lopes, L. D. de Witte, S. Debette, J. Deckert, T. Del Ser, N. Denning, A. DeStefano, M. Dichgans, J. Diehl-Schmid, M. Diez-Fairen, P. D. Rossi, S. Djurovic, E. Duron, E. Düzel, C. Dufouil, G. Eiriksdottir, S. Engelborghs, V. Escott-Price, A. Espinosa, M. Ewers, K. M. Faber, T. Fabrizio, S. F. Nielsen, D. W. Fardo, L. Farotti, C. Fenoglio, M. Fernández-Fuertes, R. Ferrari, C. B. Ferreira, E. Ferri, B. Fin, P. Fischer, T. Fladby, K. Fließbach, B. Fongang, M. Fornage, J. Fortea, T. M. Foroud, S. Fostinelli, N. C. Fox, E. Franco-Macías, M. J. Bullido, A. Frank-García, L. Froelich, B. Fulton-Howard, D. Galimberti, J. M. García-Alberca, P. García-González, S. Garcia-Madrona, G. Garcia-Ribas, R. Ghidoni, I. Giegling, G. Giorgio, A. M. Goate, O. Goldhardt, D. Gomez-Fonseca, A. González-Pérez, C. Graff, G. Grande, E. Green, T. Grimmer, E. Grünblatt, M. Grunin, V. Gudnason, T. Guetta-Baranes, A. Haapasalo, G. Hadjigeorgiou, J. L. Haines, K. L. Hamilton-Nelson, H. Hampel, O. Hanon, J. Hardy, A. M. Hartmann, L. Hausner, J. Harwood, S. Heilmann-Heimbach, S. Helisalmi, M. T. Heneka, I. Hernández, M. J. Herrmann, P. Hoffmann, C. Holmes, H. Holstege, R. H. Vilas, M. Hulsman, J. Humphrey, G. J. Biessels, X. Jian, C. Johansson, G. R. Jun, Y. Kastumata, J. Kauwe, P. G. Kehoe, L. Kilander, A. K. Ståhlbom, M. Kivipelto, A. Koivisto, J. Kornhuber, M. H. Kosmidis, W. A. Kukull, P. P. Kuksa, B. W. Kunkle, A. B. Kuzma, C. Lage, E. J. Laukka, L. Launer, A. Lauria, C.-Y. Lee, J. Lehtisalo, O. Lerch, A. Lleó, W. Longstreth, O. Lopez, A. L. de Munain, S. Love, M. Löwemark, L. Luckcuck, K. L. Lunetta, Y. Ma, J. Macías, C. A. MacLeod, W. Maier, F. Mangialasche, M. Spallazzi, M. Marquié, R. Marshall, E. R. Martin, A. M. Montes, C. M. Rodríguez, C. Masullo, R. Mayeux, S. Mead, P. Mecocci, M. Medina, A. Meggy, S. Mehrabian, S. Mendoza, M. Menéndez-González, P. Mir, S. Moebus, M. Mol, L. Molina-Porcel, L. Montrreal, L. Morelli, F. Moreno, K. Morgan, T. Mosley, M. M. Nöthen, C. Muchnik, S. Mukherjee, B. Nacmias, T. Ngandu,

G. Nicolas, B. G. Nordestgaard, R. Olaso, A. Orellana, M. Orsini, G. Ortega, A. Padovani, C. Paolo, G. Papenberg, L. Parnetti, F. Pasquier, P. Pastor, G. Peloso, A. Pérez-Cordón, J. Pérez-Tur, P. Pericard, O. Peters, Y. A. L. Pijnenburg, J. A. Pineda, G. Piñol-Ripoll, C. Pisanu, T. Polak, J. Popp, D. Posthuma, J. Priller, R. Puerta, O. Quenez, I. Quintela, J. Q. Thomassen, A. Rábano, I. Rainero, F. Rajabli, I. Ramakers, L. M. Real, M. J. T. Reinders, C. Reitz, D. Reyes-Dumeyer, P. Ridge, S. Riedel-Heller, P. Riederer, N. Roberto, E. Rodriguez-Rodriguez, A. Rongve, I. R. Allende, M. Rosende-Roca, J. L. Royo, E. Rubino, D. Rujescu, M. E. Sáez, P. Sakka, I. Saltvedt, Á. Sanabria, M. B. Sánchez-Arjona, F. Sanchez-Garcia, P. S. Juan, R. Sánchez-Valle, S. B. Sando, C. Sarnowski, C. L. Satizabal, M. Scamosci, N. Scarmeas, E. Scarpini, P. Scheltens, N. Scherbaum, M. Scherer, M. Schmid, A. Schneider, J. M. Schott, G. Selbæk, D. Seripa, M. Serrano, J. Sha, A. A. Shadrin, O. Skrobot, S. Slifer, G. J. L. Snijders, H. Soininen, V. Solfrizzi, A. Solomon, Y. Song, S. Sorbi, O. Sotolongo-Grau, G. Spalletta, A. Spottke, A. Squassina, E. Stordal, J. P. Tartan, L. Tárraga, N. Tesí, A. Thalamuthu, T. Thomas, G. Tosto, L. Traykov, L. Tremolizzo, A. Tybjærg-Hansen, A. Uitterlinden, A. Ullgren, I. Ulstein, S. Valero, O. Valladares, C. V. Broeckhoven, J. Vance, B. N. Vardarajan, A. van der Lugt, J. V. Dongen, J. van Rooij, J. van Swieten, R. Vandenberghe, F. Verhey, J.-S. Vidal, J. Vogelgsang, M. Vyhnalek, M. Wagner, D. Wallon, L.-S. Wang, R. Wang, L. Weinhold, J. Wiltfang, G. Windle, B. Woods, M. Yannakoulia, H. Zare, Y. Zhao, X. Zhang, C. Zhu, M. Zulaica, EADB, GR@ACE, DEGESCO, EADI, GERAD, Demgene, FinnGen, ADGC, CHARGE, L. A. Farrer, B. M. Psaty, M. Ghanbari, T. Raj, P. Sachdev, K. Mather, F. Jessen, M. A. Ikram, A. de Mendonça, J. Hort, M. Tsolaki, M. A. Pericak-Vance, P. Amouyel, J. Williams, R. Frikke-Schmidt, J. Clarimon, J.-F. Deleuze, G. Rossi, S. Seshadri, O. A. Andreassen, M. Ingelsson, M. Hiltunen, K. Sleegers, G. D. Schellenberg, C. M. van Duijn, R. Sims, W. M. van der Flier, A. Ruiz, A. Ramirez, J.-C. Lambert, New insights into the genetic etiology of Alzheimer's disease and related dementias. *Nat Genet* (2022), doi:10.1038/s41588-022-01024-z.

16. L. Brase, S.-F. You, R. D. Albanus, J. L. Del-Aguila, Y. Dai, B. C. Novotny, C. Soriano-Tarraga, T. Dykstra, M. V. Fernandez, J. P. Budde, K. Bergmann, J. C. Morris, R. J. Bateman, R. J. Perrin, E. McDade, C. Xiong, A. Goate, M. Farlow, J. P. Chhatwal, P. Schofield, H. Chui, Dominantly Inherited Alzheimer Network (DIAN), G. T. Sutherland, J. Kipnis, C. M. Karch, B. A. Benitez, C. Cruchaga, O. Harari, "A landscape of the genetic and cellular heterogeneity in Alzheimer disease" (preprint, Neurology, 2021), , doi:10.1101/2021.11.30.21267072.

17. M. Olah, V. Menon, N. Habib, M. F. Taga, Y. Ma, C. J. Yung, M. Cimpean, A. Khairallah, G. Coronas-Samano, R. Sankowski, D. Grün, A. A. Kroshilina, D. Dionne, R. A. Sarkis, G. R. Cosgrove, J. Helgager, J. A. Golden, P. B. Pennell, M. Prinz, J. P. G. Vonsattel, A. F. Teich, J. A. Schneider, D. A. Bennett, A. Regev, W. Elyaman, E. M. Bradshaw, P. L. De Jager, Single cell RNA sequencing of human microglia uncovers a subset associated with Alzheimer's disease. *Nat Commun*. **11**, 6129 (2020).

18. S.-F. Lau, H. Cao, A. K. Y. Fu, N. Y. Ip, Single-nucleus transcriptome analysis reveals dysregulation of angiogenic endothelial cells and neuroprotective glia in Alzheimer's disease. *Proc Natl Acad Sci U S A*. **117**, 25800–25809 (2020).

19. S. Morabito, E. Miyoshi, N. Michael, S. Shahin, A. C. Martini, E. Head, J. Silva, K. Leavy, M. Perez-Rosendahl, V. Swarup, Single-nucleus chromatin accessibility and transcriptomic characterization of Alzheimer's disease. *Nat Genet* (2021), doi:10.1038/s41588-021-00894-z.

20. N. M. Dräger, S. M. Sattler, C. T.-L. Huang, O. M. Teter, K. Leng, S. H. Hashemi, J. Hong, C. D. Clelland, L. Zhan, L. Kodama, A. B. Singleton, M. A. Nalls, J. Ichida, M. E. Ward, F. Faghri, L. Gan, M. Kampmann, "A CRISPRi/a platform in iPSC-derived microglia uncovers regulators of disease states" (preprint, Neuroscience, 2021), , doi:10.1101/2021.06.16.448639.

21. Q. Li, B. A. Barres, Microglia and macrophages in brain homeostasis and disease. *Nat Rev Immunol*. **18**, 225–242 (2018).

22. A. Kumanogoh, H. Kikutani, Immunological functions of the neuropilins and plexins as receptors for semaphorins. *Nat Rev Immunol*. **13**, 802–814 (2013).

23. G. Jun, H. Asai, E. Zeldich, E. Drapeau, C. Chen, J. Chung, J.-H. Park, S. Kim, V. Haroutunian, T. Foroud, R. Kuwano, J. L. Haines, M. A. Pericak-Vance, G. D. Schellenberg, K. L. Lunetta, J.-W. Kim, J. D. Buxbaum, R. Mayeux, T. Ikezu, C. R. Abraham, L. A. Farrer, PLXNA4 is associated with Alzheimer disease and modulates tau phosphorylation. *Ann Neurol*. **76**, 379–392 (2014).

24. P. F. Good, D. Alapat, A. Hsu, C. Chu, D. Perl, X. Wen, D. E. Burstein, D. S. Kohtz, A role for semaphorin 3A signaling in the degeneration of hippocampal neurons during Alzheimer's disease. *J Neurochem*. **91**, 716–736 (2004).

25. M. Efremova, M. Vento-Tormo, S. A. Teichmann, R. Vento-Tormo, CellPhoneDB: inferring cell–cell communication from combined expression of multi-subunit ligand–receptor complexes. *Nat Protoc*. **15**, 1484–1506 (2020).

26. Y. Zhou, W. M. Song, P. S. Andhey, A. Swain, T. Levy, K. R. Miller, P. L. Poliani, M. Cominelli, S. Grover, S. Gilfillan, M. Cella, T. K. Ulland, K. Zaitsev, A. Miyashita, T. Ikeuchi, M. Sainouchi, A. Kakita, D. A. Bennett, J. A. Schneider, M. R. Nichols, S. A. Beausoleil, J. D. Ulrich, D. M. Holtzman, M. N. Artyomov, M. Colonna, Human and mouse single-nucleus transcriptomics reveal TREM2-dependent and TREM2-independent cellular responses in Alzheimer's disease. *Nat Med*. **26**, 131–142 (2020).

27. Y. Hu, T. Peng, L. Gao, K. Tan, CytoTalk: De novo construction of signal transduction networks using single-cell transcriptomic data. *Sci. Adv.* **7**, eabf1356 (2021).

28. Z. Szepesi, O. Manouchehrian, S. Bachiller, T. Deierborg, Bidirectional Microglia-Neuron Communication in Health and Disease. *Front Cell Neurosci*. **12**, 323 (2018).

29. F. Nakamura, R. G. Kalb, S. M. Strittmatter, Molecular basis of semaphorin-mediated axon guidance. *J Neurobiol*. **44**, 219–229 (2000).

30. J. Klesney-Tait, I. R. Turnbull, M. Colonna, The TREM receptor family and signal integration. *Nat Immunol*. **7**, 1266–1273 (2006).

31. D. L. Kober, T. J. Brett, TREM2-Ligand Interactions in Health and Disease. *J Mol Biol*. **429**, 1607–1629 (2017).

32. E. E. Evans, V. Mishra, C. Mallow, E. M. Gersz, L. Balch, A. Howell, C. Reilly, E. S. Smith, T. L. Fisher, M. Zauderer, Semaphorin 4D is up-regulated in neurons of diseased brains and triggers astrocyte reactivity. *J Neuroinflammation*. **19**, 200 (2022).

33. T. K. Ulland, M. Colonna, TREM2 — a key player in microglial biology and Alzheimer disease. *Nat Rev Neurol*. **14**, 667–675 (2018).

34. Y. Atagi, C.-C. Liu, M. M. Painter, X.-F. Chen, C. Verbeeck, H. Zheng, X. Li, R. Rademakers, S. S. Kang, H. Xu, S. Younkin, P. Das, J. D. Fryer, G. Bu, Apolipoprotein E Is a Ligand for Triggering Receptor Expressed on Myeloid Cells 2 (TREM2). *J Biol Chem*. **290**, 26043–26050 (2015).

35. F. L. Yeh, Y. Wang, I. Tom, L. C. Gonzalez, M. Sheng, TREM2 Binds to Apolipoproteins, Including APOE and CLU/APOJ, and Thereby Facilitates Uptake of Amyloid-Beta by Microglia. *Neuron*. **91**, 328–340 (2016).

36. S. M. Neuner, J. Tcw, A. M. Goate, Genetic architecture of Alzheimer's disease. *Neurobiol Dis*. **143**, 104976 (2020).

37. E. Rogaeva, Y. Meng, J. H. Lee, Y. Gu, T. Kawarai, F. Zou, T. Katayama, C. T. Baldwin, R. Cheng, H. Hasegawa, F. Chen, N. Shibata, K. L. Lunetta, R. Pardossi-Piquard, C. Bohm, Y. Wakutani, L. A. Cupples, K. T. Cuenco, R. C. Green, L. Pinessi, I. Rainero, S. Sorbi, A. Bruni, R. Duara, R. P. Friedland, R. Inzelberg, W. Hampe, H. Bujo, Y.-Q. Song, O. M. Andersen, T. E. Willnow, N. Graff-Radford, R. C. Petersen, D. Dickson, S. D. Der, P. E. Fraser, G. Schmitt-Ulms, S. Younkin, R. Mayeux, L. A. Farrer, P. St George-Hyslop, The neuronal sortilin-related receptor SORL1 is genetically associated with Alzheimer disease. *Nat Genet*. **39**, 168–177 (2007).

38. R.-H. Yin, J.-T. Yu, L. Tan, The Role of SORL1 in Alzheimer's Disease. *Mol Neurobiol*. **51**, 909–918 (2015).

39. Y. Deming, F. Filipello, F. Cignarella, C. Cantoni, S. Hsu, R. Mikesell, Z. Li, J. L. Del-Aguila, U. Dube, F. G. Farias, J. Bradley, J. Budde, L. Ibanez, M. V. Fernandez, K. Blennow, H. Zetterberg, A. Heslegrave, P. M. Johansson, J. Svensson, B. Nellgård, A. Lleo, D. Alcolea, J. Clarimon, L. Rami, J. L. Molinuevo, M. Suárez-Calvet, E. Morenas-Rodríguez, G. Kleinberger, M. Ewers, O. Harari, C. Haass, T. J. Brett, B. A. Benitez, C. M. Karch, L. Piccio, C. Cruchaga, The MS4A gene cluster is a key modulator of soluble TREM2 and Alzheimer's disease risk. *Sci Transl Med*. **11**, eaau2291 (2019).

40. W.-Y. Wang, M.-S. Tan, J.-T. Yu, L. Tan, Role of pro-inflammatory cytokines released from microglia in Alzheimer's disease. *Ann Transl Med*. **3**, 136 (2015).

41. A. McQuade, M. Coburn, C. H. Tu, J. Hasselmann, H. Davtyan, M. Blurton-Jones, Development and validation of a simplified method to generate human microglia from pluripotent stem cells. *Mol Neurodegener*. **13**, 67 (2018).

42. T. R. Jay, V. E. von Saucken, G. E. Landreth, TREM2 in Neurodegenerative Diseases. *Mol Neurodegener*. **12**, 56 (2017).

43. A. Grubman, X. Y. Choo, G. Chew, J. F. Ouyang, G. Sun, N. P. Croft, F. J. Rossello, R. Simmons, S. Buckberry, D. V. Landin, J. Pflueger, T. H. Vandekolk, Z. Abay, Y. Zhou, X. Liu, J. Chen, M. Larcombe, J. M. Haynes, C. McLean, S. Williams, S. Y. Chai, T. Wilson, R. Lister, C. W. Pouton, A. W. Purcell, O. J. L. Rackham, E. Petretto, J. M. Polo, Transcriptional signature in microglia associated with Aβ plaque phagocytosis. *Nat Commun*. **12**, 3015 (2021).

44. A. McQuade, Y. J. Kang, J. Hasselmann, A. Jairaman, A. Sotelo, M. Coburn, S. K. Shabestari, J. P. Chadarevian, G. Fote, C. H. Tu, E. Danhash, J. Silva, E. Martinez, C. Cotman, G. A. Prieto, L. M. Thompson, J. S. Steffan, I. Smith, H. Davtyan, M. Cahalan, H. Cho, M. Blurton-Jones, Gene expression and functional deficits underlie TREM2-knockout microglia responses in human models of Alzheimer's disease. *Nat Commun*. **11**, 5370 (2020).

45. H. Keren-Shaul, A. Spinrad, A. Weiner, O. Matcovitch-Natan, R. Dvir-Szternfeld, T. K. Ulland, E. David, K. Baruch, D. Lara-Astaiso, B. Toth, S. Itzkovitz, M. Colonna, M. Schwartz, I. Amit, A Unique Microglia Type Associated with Restricting Development of Alzheimer's Disease. *Cell*. **169**, 1276-1290.e17 (2017).

46. N. Takegahara, H. Takamatsu, T. Toyofuku, T. Tsujimura, T. Okuno, K. Yukawa, M. Mizui, M. Yamamoto, D. V. R. Prasad, K. Suzuki, M. Ishii, K. Terai, M. Moriya, Y. Nakatsuji, S. Sakoda, Plexin-A1 and its interaction with DAP12 in immune responses and bone homeostasis. *Nature Cell Biology*. **8**, 615–22 (2006).

47. A. Kumanogoh, H. Kikutani, Immunological functions of the neuropilins and plexins as receptors for semaphorins. *Nature Reviews. Immunology*. **13**, 802–14 (2013).

48. S. S. Kang, A. Kurti, A. Wojtas, K. E. Baker, C.-C. Liu, T. Kanekiyo, Y. Deming, C. Cruchaga, S. Estus, G. Bu, J. D. Fryer, Identification of plexin A4 as a novel clusterin receptor links two Alzheimer's disease risk genes. *Hum Mol Genet*. **25**, 3467–3475 (2016).

49. Q. Han, Y.-A. Sun, Y. Zong, C. Chen, H.-F. Wang, L. Tan, Alzheimer's Disease Neuroimaging Initiative, Common Variants in PLXNA4 and Correlation to CSF-related Phenotypes in Alzheimer's Disease. *Frontiers in Neuroscience*. **12** (2018) (available at https://www.frontiersin.org/articles/10.3389/fnins.2018.00946).

50. S. Chung, J. Yang, H. J. Kim, E. M. Hwang, W. Lee, K. Suh, H. Choi, I. Mook-Jung, Plexin-A4 mediates amyloid-β-induced tau pathology in Alzheimer's disease animal model. *Prog Neurobiol*. **203**, 102075 (2021).

51. A. Macedo, C. Gómez, M. Â. Rebelo, J. Poza, I. Gomes, S. Martins, A. Maturana-Candelas, V. G. Pablo, L. Durães, P. Sousa, M. Figueruelo, M. Rodríguez, C. Pita, M. Arenas, L. Álvarez, R. Hornero, A. M. Lopes, N. Pinto, Risk Variants in Three Alzheimer's Disease Genes Show Association with EEG Endophenotypes. *J Alzheimers Dis*. **80**, 209–223 (2021).

52. Y. Deming, Z. Li, M. Kapoor, O. Harari, J. L. Del-Aguila, K. Black, D. Carrell, Y. Cai, M. V. Fernandez, J. Budde, S. Ma, B. Saef, B. Howells, K.-L. Huang, S. Bertelsen, A. M. Fagan, D. M. Holtzman, J. C. Morris, S. Kim, A. J. Saykin, P. L. De Jager, M. Albert, A. Moghekar, R. O'Brien, M. Riemenschneider, R. C. Petersen, K. Blennow, H. Zetterberg, L. Minthon, V. M. Van Deerlin, V. M.-Y. Lee, L. M. Shaw, J. Q. Trojanowski, G. Schellenberg, J. L. Haines, R. Mayeux, M. A. Pericak-Vance, L. A. Farrer, E. R. Peskind, G. Li, A. F. Di Narzo, Alzheimer's Disease Neuroimaging Initiative (ADNI), Alzheimer Disease Genetic Consortium (ADGC), J. S. K. Kauwe, A. M. Goate, C. Cruchaga, Genome-wide association study identifies four novel loci associated with Alzheimer's endophenotypes and disease modifiers. *Acta Neuropathol*. **133**, 839–856 (2017).

53. A. Zettergren, K. Höglund, S. Kern, V. Thorvaldsson, M. Johan Skoog, O. Hansson, N. Andreasen, N. Bogdanovic, K. Blennow, I. Skoog, H. Zetterberg, Association of IL1RAP-related genetic variation with cerebrospinal fluid concentration of Alzheimer-associated tau protein. *Sci Rep*. **9**, 2460 (2019).

54. F. Su, F. Bai, Z. Zhang, Inflammatory Cytokines and Alzheimer's Disease: A Review from the Perspective of Genetic Polymorphisms. *Neurosci Bull*. **32**, 469–480 (2016).

55. G. Ogunmokun, S. Dewanjee, P. Chakraborty, C. Valupadas, A. Chaudhary, V. Kolli, U. Anand, J. Vallamkondu, P. Goel, H. P. R. Paluru, K. D. Gill, P. H. Reddy, V. De Feo, R. Kandimalla, The Potential Role of Cytokines and Growth Factors in the Pathogenesis of Alzheimer's Disease. *Cells*. **10**, 2790 (2021).

56. A. S. Mendiola, A. E. Cardona, The IL-1β phenomena in neuroinflammatory diseases. *J Neural Transm (Vienna)*. **125**, 781–795 (2018).

57. T. Stuart, A. Butler, P. Hoffman, C. Hafemeister, E. Papalexi, W. M. Mauck, Y. Hao, M. Stoeckius, P. Smibert, R. Satija, Comprehensive Integration of Single-Cell Data. *Cell*. **177**, 1888-1902.e21 (2019).

58. C. Hafemeister, R. Satija, Normalization and variance stabilization of single-cell RNA-seq data using regularized negative binomial regression. *Genome Biol*. **20**, 296 (2019).

59. Y. Zhang, T. Liu, C. A. Meyer, J. Eeckhoute, D. S. Johnson, B. E. Bernstein, C. Nussbaum, R. M. Myers, M. Brown, W. Li, X. S. Liu, Model-based Analysis of ChIP-Seq (MACS). *Genome Biol*. **9**, R137 (2008).

60. H. M. Amemiya, A. Kundaje, A. P. Boyle, The ENCODE Blacklist: Identification of Problematic Regions of the Genome. *Sci Rep*. **9**, 9354 (2019).

61. H. A. Pliner, J. S. Packer, J. L. McFaline-Figueroa, D. A. Cusanovich, R. M. Daza, D. Aghamirzaie, S. Srivatsan, X. Qiu, D. Jackson, A. Minkina, A. C. Adey, F. J. Steemers, J. Shendure, C. Trapnell, Cicero Predicts cis-Regulatory DNA Interactions from Single-Cell Chromatin Accessibility Data. *Mol. Cell*. **71**, 858-871.e8 (2018).

62. A. Patel, A. Garcia Diaz, J. C. Moore, D. Sirabella, B. Corneo, Establishment and characterization of two iPSC lines derived from healthy controls. *Stem Cell Res*. **47**, 101926 (2020).

63. W. B. Stine, K. N. Dahlgren, G. A. Krafft, M. J. LaDu, In vitro characterization of conditions for amyloid-beta peptide oligomerization and fibrillogenesis. *J Biol Chem*. **278**, 11612–11622 (2003).

64. D. Kim, J. M. Paggi, C. Park, C. Bennett, S. L. Salzberg, Graph-based genome alignment and genotyping with HISAT2 and HISAT-genotype. *Nat Biotechnol*. **37**, 907–915 (2019).

65. M. I. Love, W. Huber, S. Anders, Moderated estimation of fold change and dispersion for RNA-seq data with DESeq2. *Genome Biol*. **15**, 550 (2014).

66. Y. Benjamini, Y. Hochberg, Controlling the False Discovery Rate: A Practical and Powerful Approach to Multiple Testing. *Journal of the Royal Statistical Society: Series B (Methodological)*. **57**, 289–300 (1995).

67. D. Szklarczyk, A. L. Gable, K. C. Nastou, D. Lyon, R. Kirsch, S. Pyysalo, N. T. Doncheva, M. Legeay, T. Fang, P. Bork, L. J. Jensen, C. von Mering, The STRING database in 2021: customizable protein-protein networks, and functional characterization of user-uploaded gene/measurement sets. *Nucleic Acids Res*. **49**, D605–D612 (2021).

68. P. Shannon, A. Markiel, O. Ozier, N. S. Baliga, J. T. Wang, D. Ramage, N. Amin, B. Schwikowski, T. Ideker, Cytoscape: a software environment for integrated models of biomolecular interaction networks. *Genome Res*. **13**, 2498–2504 (2003).

69. J. H. Morris, L. Apeltsin, A. M. Newman, J. Baumbach, T. Wittkop, G. Su, G. D. Bader, T. E. Ferrin, clusterMaker: a multi-algorithm clustering plugin for Cytoscape. *BMC Bioinformatics*. **12**, 436 (2011).

70. C. E. Shannon, A Mathematical Theory of Communication. *Bell System Technical Journal*. **27**, 379–423 (1948).

71. A. A. Margolin, I. Nemenman, K. Basso, C. Wiggins, G. Stolovitzky, R. Dalla Favera, A. Califano, ARACNE: an algorithm for the reconstruction of gene regulatory networks in a mammalian cellular context. *BMC Bioinformatics*. **7 Suppl 1**, S7 (2006).

72. P. Langfelder, S. Horvath, WGCNA: an R package for weighted correlation network analysis. *BMC Bioinformatics*. **9**, 559 (2008).

Methods

snRNA-seq data processing

Our single-nucleus RNA-seq dataset from 67 donors was processed as described previously (*16*). Briefly, we used the 10X Chromium single-cell Reagent Kit v3 aiming for 10,000 nuclei per individual and 50,000 reads per nucleus. We mapped the sequenced reads to the GRCh38 human reference genome using CellRanger (v. 6.1.1) and filtered nuclei based on sequencing depth and percent mitochondrial reads. In total, we obtained snRNA-seq data from 294,114 nuclei after stringent QC. We used Seurat (*57*) (v. 3.2.3) to identify cell types and transcriptional states.

We obtained the count matrices and barcode metadata from other public snRNA-seq datasets from human brains (*18*, *19*, *26*) as made available by the authors. We used the barcode metadata to annotate the nuclei into cell types and donor categories. We considered any nuclei not in the final metadata table for the respective study as failing QC. These nuclei were discarded from downstream analyses. In order to run CellPhoneDB and CytoTalk in these datasets, we normalized each study separately using the SCT normalization (*58*) from Seurat.

Reanalysis of brain snATAC-seq data

We downloaded the raw snATAC-seq fastq files from the Morabito *et al.* study (*19*) and re-processed this dataset using CellRanger-ATAC (v. 2.0.0) count function. Firstly, we filtered the resulting GRCh38 BAM files for each sample using flags *-f 3 -F 4 -F 8 -F 256 -F 1024 -F 2048 -q 30* to retain high-quality, properly mapped alignments. Second, we split each sample BAM file into separate files corresponding to each cell type using the barcode annotations reported by the study authors. For each cell type, we merged all BAM files across donors and called narrow peaks using MACS2 (v. 2.2.7.1) (*59*) using flags *--nomodel --shift -100 --extsize 200 --keep-dup all --call-summits -B*. Third, we filtered all peaks that overlapped the GRCh38 ENCODE exclusion list regions (ENCODE accession ENCFF356LFX) (*60*). Finally, we used CICERO (*61*), with default parameters, to calculate co-accessibility across ATAC-seq narrow peaks for each cell type separately.

Cell Culture

iPSCs were maintained feeder-free on matrigel-coated plates in StemFlex medium (Gibco) in a humidified incubator (5% CO_2, 37 °C).

Differentiation of iPSC to iPSC-derived microglia (iMGL)

iPSC-microglia were generated as described in McQuade et al., 2018 (*41*). Briefly, iPSCs were directed down a hematopoietic lineage using the STEMdiff Hematopoietic kit (STEMCELL Technologies). After 12 days in culture, hematopoietic progenitor cells (HPCs) were transferred into a microglia differentiation medium containing DMEM/F12, 2× insulin-transferrin-selenite, 2× B27, 0.5× N2, 1× GlutaMAX, 1× nonessential amino acids, 400 μM monothioglycerol, and 5 μg/mL human insulin. Media was added to cultures every other day and supplemented with 100 ng/mL IL-34, 50 ng/mL TGF-β1, and 25 ng/mL M-CSF (PeproTech) for 28 days. In the final three days of differentiation, 100 ng/mL CD200 (Novoprotein) and 100 ng/mL CX3CL1 (PeproTech) were added to the culture.

Generation of TREM2 KO iPSCs

The WT iPSC line (APOE 3/3) was a generous gift from Dr. Barbara Corneo (*62*). TREM2 KO iiPSCs were generated using the Human Stem Cell Nucleofector™ Kit 2 (Lonza) according to the manufacturer's protocol. Briefly, iiPSCs were resuspended in 100 µL nucleofection buffer and 5 µg of vector lentiCRISPRv2GFP expressing sgRNA against TREM2 (5'ATCACAGACGATACCCTGGG 3'). LentiCRISPRv2GFP was a generous gift from David Feldser (Addgene plasmid# 82416; http://n2t.net/addgene:82416; RRID:Addgene_82416). The suspension was transferred to the Amaxa Nucleofector cuvette and transfected using program CA-137. GFP-expressing cells were single-cell sorted into 96-well plates using the BD Influx cell sorter (Columbia University CCTI/HICCC Flow Core). Cell colonies were maintained and expanded. TREM2 KO cell lines were verified by Sequencing (Genewiz).

Western Blotting Analysis and Antibodies

Proteins were resolved via SDS-PAGE using NuPAGE™ 4-12% Bis-Tris gels (Invitrogen) and probed for expression. Proteins were detected using the Odyssey XF Imager (LI-COR Biosciences). Antibodies used included: anti-Phospho-SYK (Cell Signaling), anti-SYK (Cell Signaling), anti-TREM2 (Cell Signaling), and anti-β-actin (Sigma).).

Immunocytochemistry

iMGL were fixed in 4% paraformaldehyde, permeabilized, and blocked for 1 hr in 10% normal goat serum or 10% fetal bovine serum. Primary antibodies were diluted in 10% normal goat serum containing 0.1% Triton X-100 and incubated overnight at 4°C. Primary antibodies included anti-TREM2 (R&D Systems), anti-IBA1 (Fujifilm), and anti-TMEM119 (Novus)). Following incubation of the primary antibody, cells were washed and incubated for 1 hr at room temperature in Alexa Fluor 568- or 488-conjugated secondary antibody (Invitrogen). Immunostained cells were mounted using VECTASHIELD Mounting Medium (Vector Laboratories) and imaged using the Nikon C1 Digital Confocal System.

Synaptosome Preparation

The human temporal lobe was homogenized using a Dounce tissue grinder in homogenization buffer (0.032 M Sucrose, 0.5 mM $CaCl_2$, 1 mM $MgCl_2$, 1 mM $NaHCO_3$ supplemented with protease/phosphatase inhibitor) and centrifuged at 1400×g. The supernatant was saved (S1), and the resulting pellet was re-homogenized in homogenization buffer and centrifuged at 700×g, resulting in supernatant, S1'. Supernatants S1 and S1' were mixed and centrifuged at 700×g resulting in supernatant, S2. S2 was centrifuged at 14000×g. The resulting pellet containing synaptosomes was resuspended in buffer (0.32 M Sucrose, 1 mM $NaHCO_3$).

Oligomer and fibril formation

Aβ42 oligomers and fibrils were prepared according to the established protocol by Stine et al. (*63*). Briefly, Aβ42 (Anaspec) was resuspended to 1 mM solution in HFIP. Aliquots were evaporated in a fume hood for 2 hrs, and the resulting peptide film was dried under vacuum in a SpeedVac and stored at -20°C. Immediately prior to use, the films were solubilized to 1 mM in anhydrous DMSO, sonicated in a bath sonicator for 10 min, and diluted to 100 µM in oligomer-

forming conditions (cold PBS; incubation at 4°C for 24 h) or fibril-forming conditions (10mM HCl; incubation at 37°C for 24 h).

pHrodo Labeling

pHrodo Red (Invitrogen) labeling protocol was adapted from the manufacturer's instructions. Briefly, Aβ42 oligomer or fibril solutions (100 µM) were centrifuged at 16000×g for 2 min to collect the aggregates. Aggregates were washed in 1 mL HBSS and centrifuged for 2 min. The supernatants were aspirated, and 200 µl of pellet aggregates were resuspended in by adding 200 µl 0.1M $NaHCO_3$ to the pellets. The pHrodo Red dye (10 mg/ml) was then added as per the manufacturer's instructions. pHrodo labeling was performed and incubated for 1 hr in the dark, followed by centrifugation at 16000×g for 2 min. Aggregates were washed 3x with HBSS and resuspended to 100 µM in HBSS.

Phagocytosis assay

iMGL were plated at a density of $3x10^5$ cells per well in 96-well plates and incubated for 24 hrs. iMGL were treated with 10 µM SEMA6D in media supplemented with either 30 µg/ml pHrodo Red tagged synaptosomes, 1 mM pHrodo Red tagged Aβ fibril or 400 nM Aβ oligomer and incubated for 24 hrs. Cells were imaged using an IncuCyte live cell imaging system. Analysis was performed by Incucyte Zoom Software. The phagocytic activity of iMGL was quantified using the Incucyte® SX5 Live-Cell Analysis instrument**.** Total cell counts were performed using the CellQuanti-Blue™ Cell Viability Assay kit (BioAssay Systems).

Cytokine assay

iMGL were plated at a density of $3x10^5$ cells per well in 96-well plates and incubated for 24 hrs. iMGL were treated with 10 µM SEMA6D for 24 hrs. Cell media was harvested, and cytokines were quantified using the V-PLEX Human Proinflammatory Panel II (4-Plex) (MSD) according to the manufacturer's instructions. Total cell counts were performed using the CellQuanti-Blue™ Cell Viability Assay kit.

iMGL RNAseq

WT or TREM2 KO iMGL were treated with 10 µM SEMA6D for 24 hrs. mRNA was extracted from iMGL using RNeasy Mini kit (Qiagen) following the manufacturer's instructions. Human mRNA sequencing and bioinformatics analysis were performed by Novogene. Raw fastq files were mapped to the GRCh38 reference genome using HISAT2 (v. 2.0.5) (*64*) and the corresponding GRCh38 index files (http://daehwankimlab.github.io/hisat2/download). We used DESeq2 (*65*) for differential analyses. Briefly, we retained genes with ≥ 10 counts in at least three samples and processed all samples together to increase the statistical power to calculate dispersion. We then retrieved the fold changes and significances for the comparisons of interest individually (*e.g.*, SEMA6D-treated WT vs. untreated WT). Finally, we adjusted for multiple testing per comparison using the Benjamini-Hochberg correction (*66*) and used a 10% false discovery rate (FDR) threshold to identify differentially expressed genes.

CellPhoneDB analyses

We used CellPhoneDB (*25*) (v. 2.1.7) to estimate crosstalk interactions based on the expression of known ligand-receptor pairs. We used the *cellphonedb method statistical_analysis* function

with default parameters to calculate crosstalk interactions at the cluster level (transcriptional state) using the sctransform-normalized snRNA-seq count matrices as input. We performed CellPhoneDB analyses for each subset of donors separately (*e.g.*, controls, sporadic AD). We considered significant all those interactions that passed multiple testing correction (Bonferroni $p < 0.05$) for the entire set of analyses (all transcriptional states and donor categories).

To address issues of potential bias from differences in cell type representation, we performed an additional CellPhoneDB analysis, downsampling each cluster in our snRNA-seq data to 100 nuclei barcodes. Similarly, we re-ran CellPhoneDB in multiple combinations of two to three cell types in our data (e.g., astrocytes and OPC only, astrocytes, microglia, and OPC only) to confirm that the resulting interactions were stable across subsets of cell types. Finally, we repeated the CellPhoneDB analyses individually for a subset of brains to confirm that the crosstalk patterns were identified at a single brain level. For other public snRNA-seq datasets analyzed in this study, we used the cluster and donor labels provided by the authors of each study.

To calculate the significance of CellPhoneDB interactions, we used Fisher exact tests (FETs) to compare the number of interactions at the cell type level. We used the union of all significant interactions across transcriptional states for each cell type. We generated one 2x2 contingency table per cell type and donor category combination for the comparisons between controls versus other donor categories. One dimension of the contingency table encoded the number of unique significant CellPhoneDB interactions involving the cell type of interest versus all other cell types combined. The other dimension encoded the number of interactions identified in the controls versus the donor category of interest. To calculate the enrichment of crosstalk interactions involving AD-related genes per cell type, we generated, for each donor category, 2x2 contingency tables encoding the number of interactions involving the cell type of interest (yes versus no) and involving AD genes (yes versus no). Finally, we calculated the enrichment of AD-related crosstalk interactions pairwise across all cell-type pairs by further subsetting the previous contingency tables to separate between AD-related interactions involving cell type of interest A and cell type of interest B versus cell type of interest A without cell type of interest B (*e.g.*, microglia and excitatory neurons versus to microglia and the remaining cell types). All FET p-values were corrected for multiple testing using the Bonferroni correction based on the total number of tests performed for each analysis.

Crosstalk enrichments for other neuropsychiatric traits

We downloaded the GWAS associations of neuropsychiatric traits from the European Bioinformatics Institute GWAS catalog (https://www.ebi.ac.uk/gwas) for the studies listed in **Supp. Table 5**. We used the mapped genes for each locus as the input gene list to calculate the crosstalk enrichments in each study. We used the same FET approach described above for the AD-related crosstalk interactions to calculate the enrichment of genes nominated by each GWAS study (Figure 2D). To calculate the enrichment of crosstalk interactions involving genes associated with AD GWAS based on co-accessibility (Figure 2E), we used as the input gene list all genes with a transcription start site (TSS) region either 1) overlapping an ATAC-seq peak co-accessible with another ATAC-seq peak harboring a fine-mapped AD GWAS variant (PPA > 0.01) from the Schwartzentruber *et al.* study (*14*) or 2) overlapping an ATAC-seq peak in any cell type harboring a fine-mapped variant.

Downstream crosstalk networks reconstruction using CytoTalk

To identify the signaling networks downstream of crosstalk interactions, we used CytoTalk (v. 4.0.3) with minor modifications. CytoTalk first reconstructs the co-expression network of two cell types using information theory, then prioritizes biologically relevant crosstalk interactions based on their connection to central genes in each network using graph theory. This analysis results in a prioritized network of genes predicted to mediate the crosstalk signals between the two cell types. Briefly, CytoTalk reconstructs the co-expression network for each cell type pair and connects them based on a database of ligand-receptor interactions. It then uses a prize-collecting Steiner forest algorithm to identify the crosstalk signaling network between the two cell types (*27*). We generated input csv files per cell type for each donor category containing the sctransform-normalized snRNA-seq log-transformed counts per barcode. Additionally, we increased the stringency of the CytoTalk networks by manually inputting only interactions that were also present in CellPhoneDB. This step was done because CytoTalk uses protein-protein interactions and text mining from STRING-DB (*67*) to build its crosstalk interactions database, which we consider overly permissive. For the network visualization in **Figure 2a**, we used the union of the crosstalk signaling network identified for each donor category in microglia versus excitatory neurons. We generated network visualizations using Cytoscape (v. 3.9.0) (*68*) and identified crosstalk sub-networks using the community cluster (GLay) function of clusterMaker (v. 2.2) (*69*). The modified CytoTalk version used in this study (https://github.com/rdalbanus/CytoTalk) fixed minor bugs and enabled better parallelization control for a cluster environment. These issues have since been fixed in newer CytoTalk releases.

To calculate the enrichment of AD-related genes downstream of the crosstalk interactions (**Figure 2c**), we used FETs to compare the number of AD-related genes in each side of the exc. neuron-microglia crosstalk network versus all AD-related genes expressed in the corresponding cell type. All FET p-values were corrected for multiple testing using the Bonferroni correction based on the total number of tests performed for each analysis.

Network analyses

We used the *compute_mutual_information_single* function from CytoTalk to reconstruct the excitatory neurons and microglia co-expression networks for each donor category. Briefly, this function calculates the mutual information (MI) (*70*) across all pairs of genes per cell type and then applies the ARACNE algorithm (*71*) to eliminate most indirect interactions between genes. We then merged the ARACNE-filtered MI matrices for each cell type across donor categories by keeping the highest MI value for each interaction. In order to identify co-expression sub-networks, we applied the WGCNA pipeline (*72*) on the merged MI matrix. To test the association of each sub-network (n = 360) with the Braak stage, we first calculated its eigengene (the first principal component of gene expression) for each sub-network. We then tested the association of each eigengene with a high Braak stage using the binomial regression model:

$$Braak\ high_i \sim eigengene_{ij} + sex_i + APOE4_i + TREM2_i$$

In this model, i represents a barcode and j, a co-expression sub-network. $Braak\ high_i$, sex_i, $APOE4_i$, and $TREM2_i$ are binary variables encoding the donor Braak stage (Braak > 3 versus

Braak ≤ 3), sex, *APOE* genotype (one or two copies of *APOE4* versus zero), and *TREM2* genotype (common variant versus R47H, R136W, or R62H). We ran this model for each sub-network and obtained the corresponding coefficient and p-value of the eigengene term. Then, we adjusted the significance for multiple testing using the Bonferroni correction. Similarly, we performed this same analysis in the sub-networks obtained from the CytoTalk microglia-exc. neurons crosstalk network.

Functional enrichments

All gene ontology (GO) functional enrichments in this study were calculated with the WebGestaltR R package (v. 0.4.4), using the *ORA* method, the *geneontology_Biological_Process_noRedundant* annotation, and the *genome_protein-coding* reference set. For all analyses, we used an FDR threshold of 1 to recover all enrichments and manually adjusted p-values for multiple testing using the Bonferroni correction (significance threshold used: $p < 0.05$). To further collapse redundancy in GO terms, we used the R package rrvgo (v. 1.9.1). For each WebGestaltR analysis, we generated a similarity matrix across all GO terms significant in at least one comparison using the *calculateSimMatrix* function. We then reduced the significant terms for each analysis using the *reduceSimMatrix* function. The *threshold* values for the *reduceSimMatrix* function were selected based on visual inspection of the resulting terms (0.8 for the analyses in Figures 1F and 3C and 0.9 for Figure 3F). Finally, we reported the most significant p-value among the grouped terms under each parent term.

Data availability

iMGL RNA-seq data will be publicly available in GEO upon publication. The snRNA-seq data from the Knight ADRC is publicly available by request from the National Institute on Aging Genetics of Alzheimer's Disease Data Storage Site (NIAGADS) under accession number NG00108 (https://www.niagads.org/datasets/ng00108). DIAN brain bank snRNA-seq data access requires a request through https://dian.wustl.edu/our-research/for-investigators.

Code availability

All scripts necessary to reproduce the figures from this manuscript will be available at https://github.com/albanus-research/2021_trem2_adad_snRNAseq. The modified CytoTalk version used for this manuscript is available at https://github.com/rdalbanus/CytoTalk.

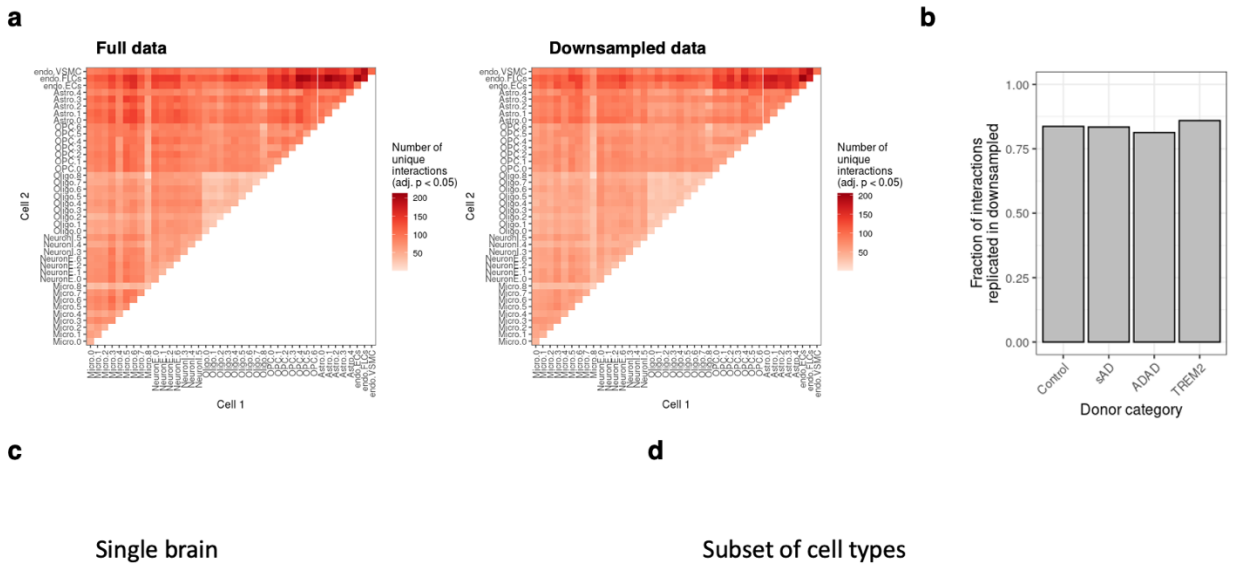

Single brain

Subset of cell types

Supplementary Figure 1. a) Overview of CellPhoneDB results on full dataset versus a heavily downsampled dataset (maximum 100 nuclei per snRNA-seq cluster). **b)** Fraction of replicated CPDB interactions in downsampled dataset compared to the full dataset.

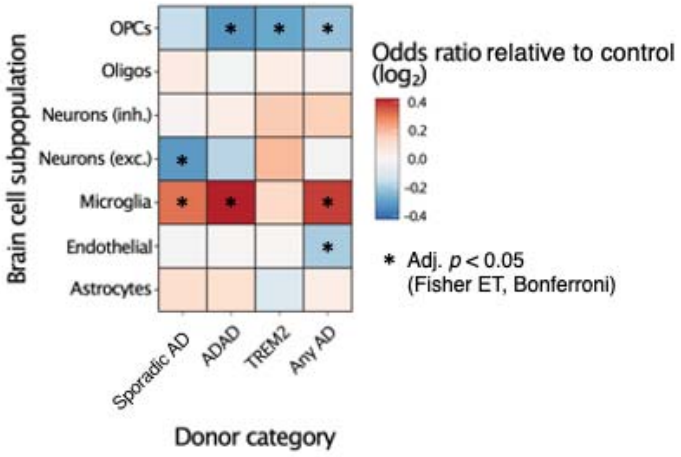

Supplementary Figure 2. Global changes in crosstalk frequencies per cell type across donor categories versus controls.

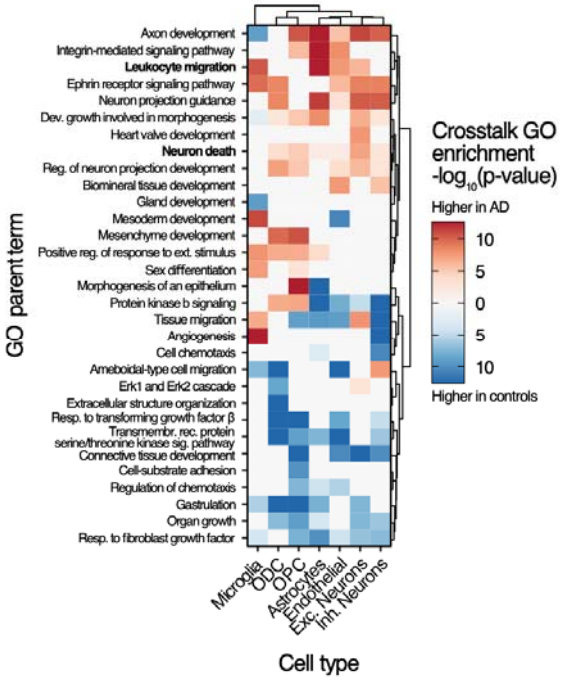

Supplementary Figure 3. Gene ontology enrichments of the genes associated with crosstalk interactions only detected in cases or controls, grouped by cell type.

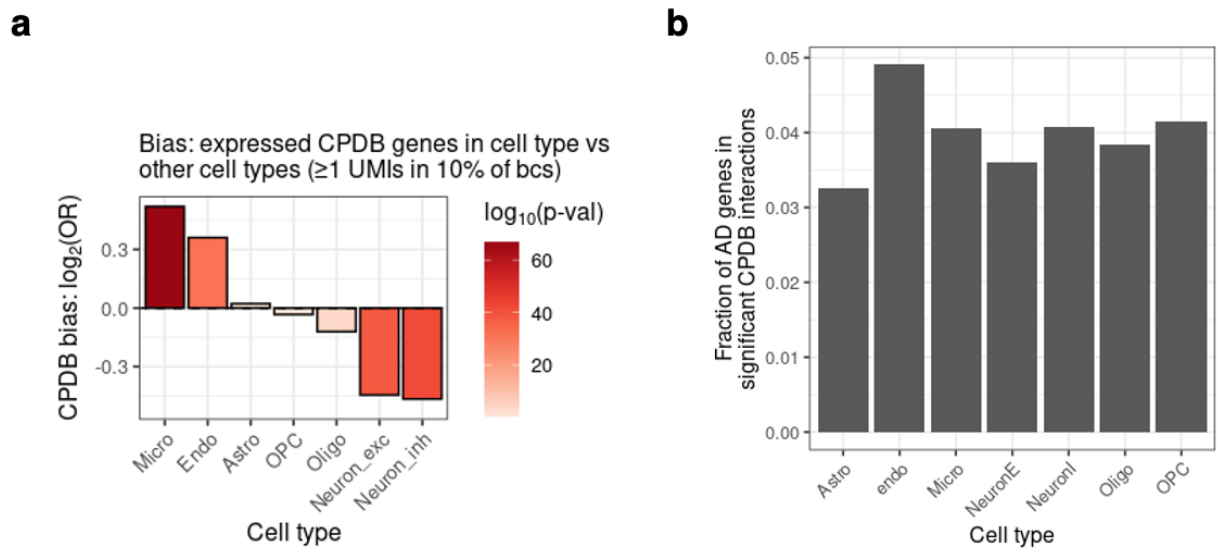

Supplementary Figure 4. a) Bias of expressed genes in each cell type belonging to a CPDB interaction. b) Fraction of AD-related genes expressed in each cell type that participate in any CPDB interaction.

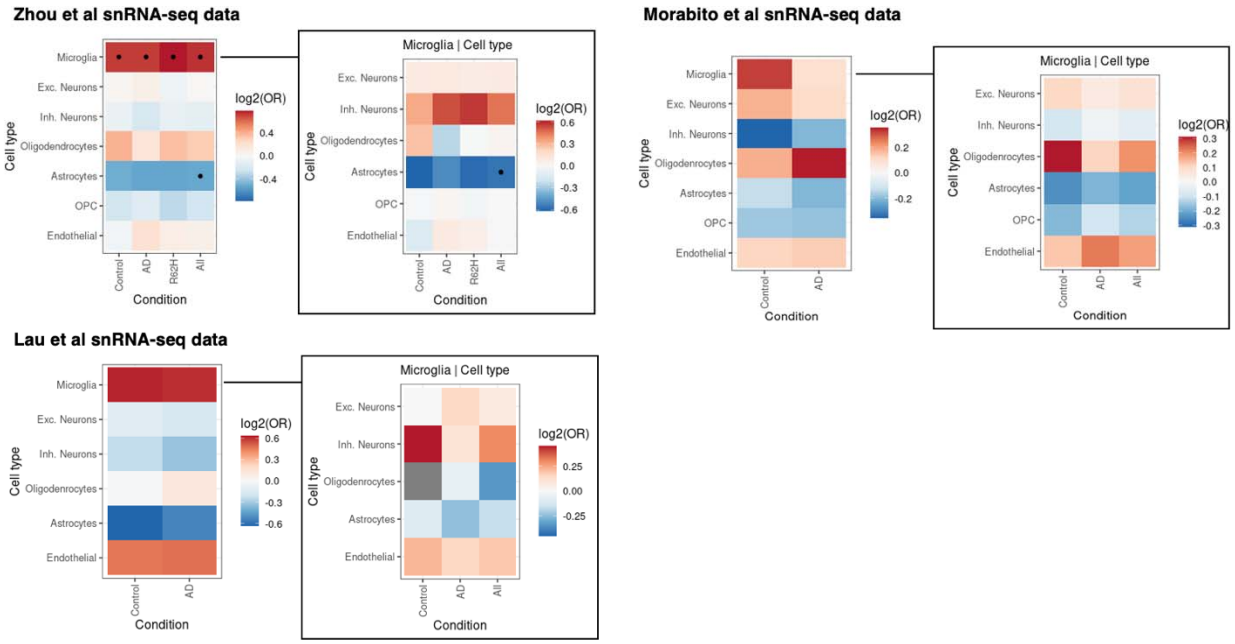

Supplementary Figure 5. Enrichment of AD crosstalk interactions involving each cell type in each donor category for different snRNA-seq datasets (left plots) and their corresponding enrichment of AD crosstalk interactions between microglia and other cell types (blowout panels).

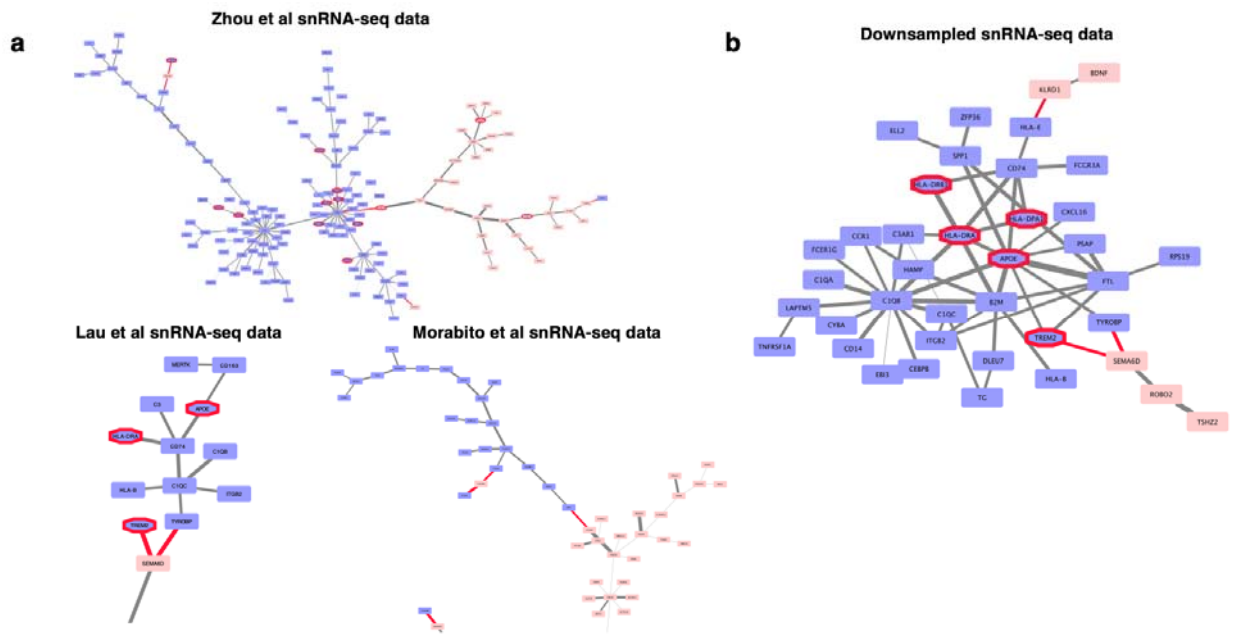

Supplementary Figure 6. a) Reconstructed exc. neurons and microglia crosstalk networks using CytoTalk in different snRNA-seq datasets. **b)** Reconstructed TREM2 crosstalk network with CytoTalk by downsampling the number of nuclei to the donor category with the smallest number of nuclei.

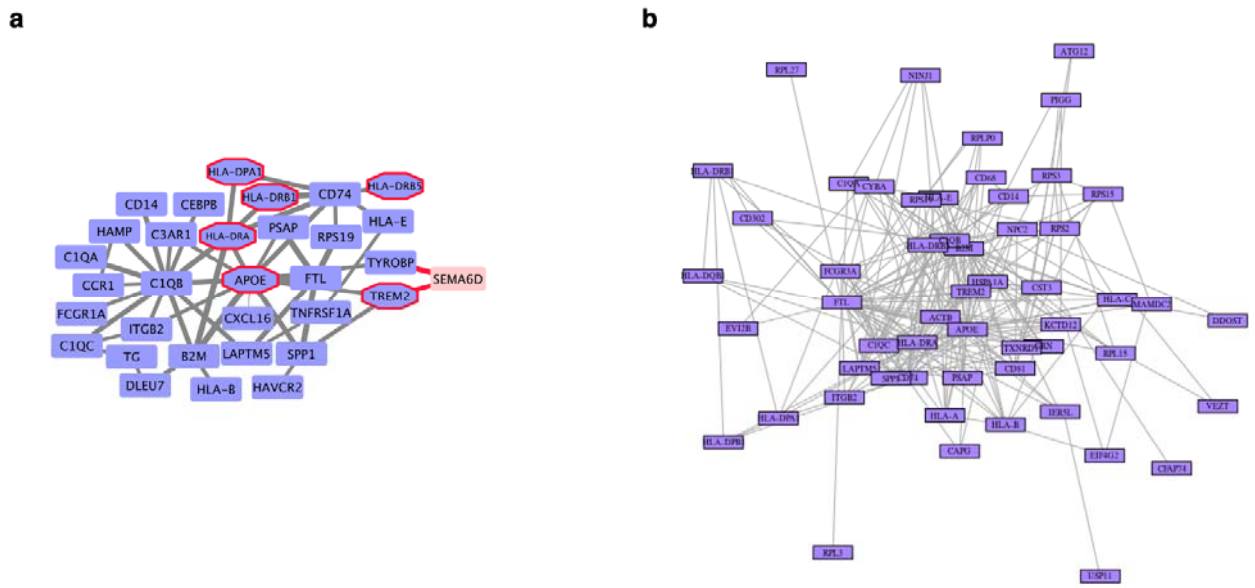

Supplementary Figure 7. Comparison of the TREM2 subnetwork prioritized by CytoTalk **(a)** and identified directly from the microglia co-expression network **(b)**.

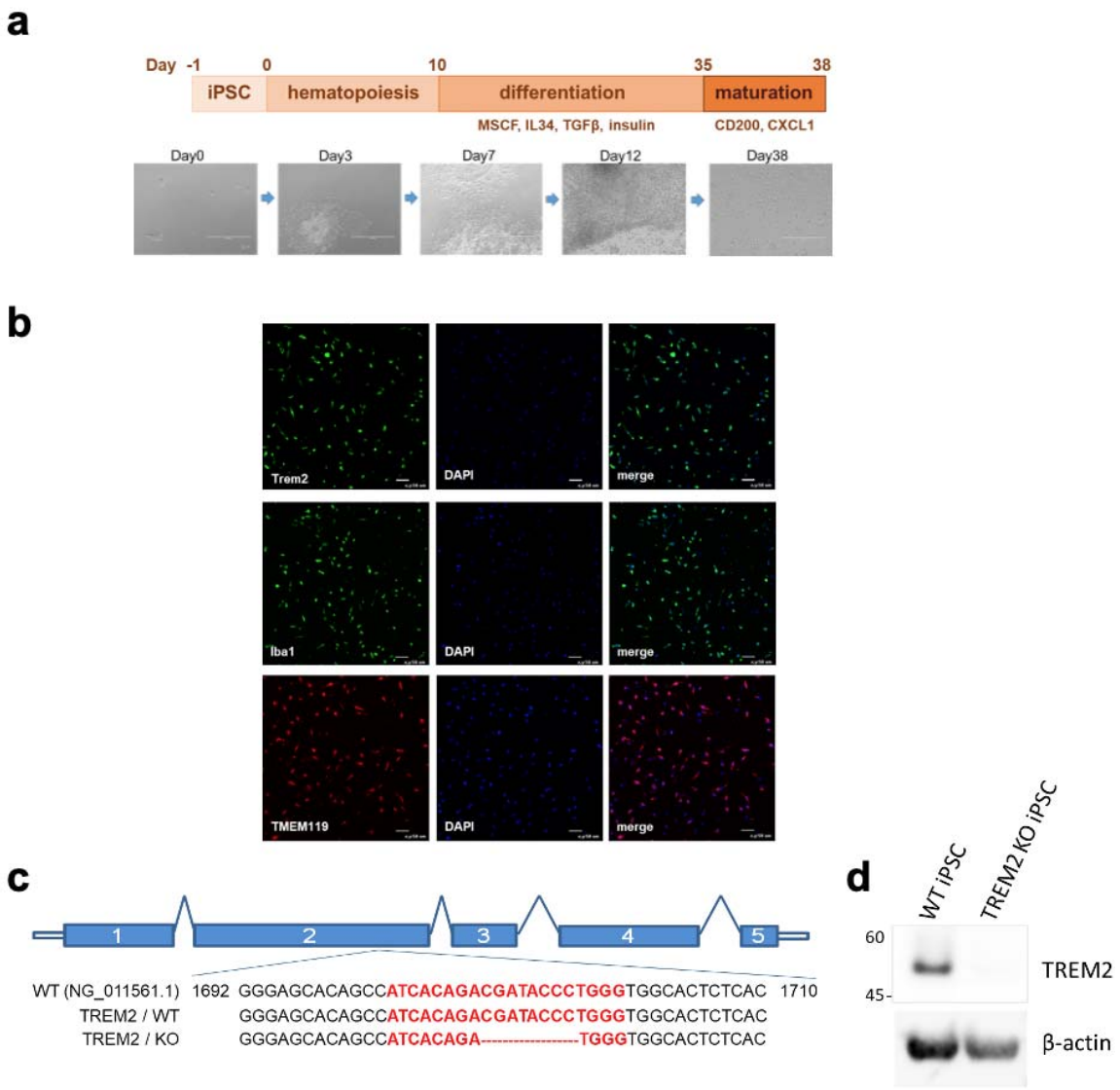

Supplementary Figure 8. a) Schematic of the differentiation procedure and brightfield imaging of iPSC-derived microglia (iMGL). **b)** mature iMGL stained with microglial markers, TREM2, Iba1, and TMEM119 and co-stained with DAPI. **c)** Schematic of DNA (red) targeted by gRNA against TREM2 for CRISPR/Cas9 modification and showing an 8 base pair homozygous deletion within exon 2 of the TREM2 gene. **d)** Western blot analysis of wild-type (WT) and TREM2 KO iPS cell lysates immunostained for TREM2 with β-actin as the loading control.

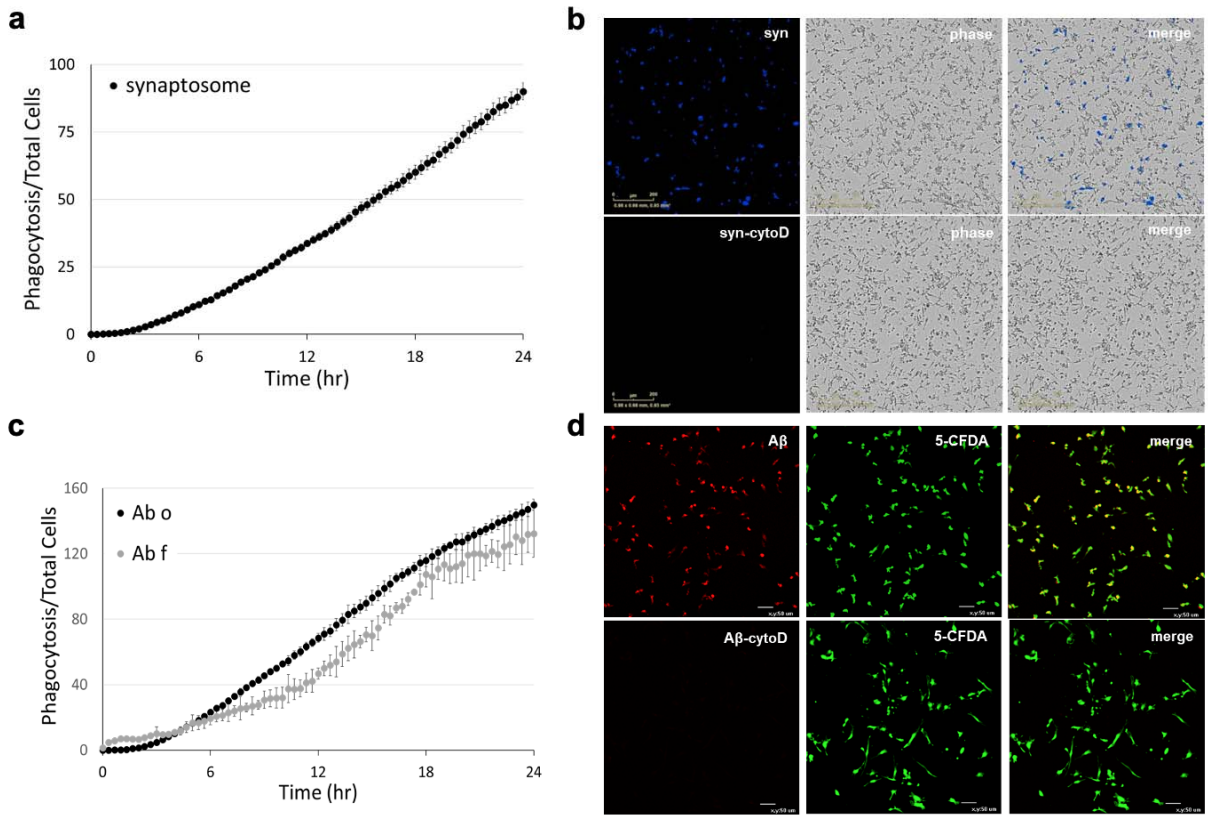

Supplementary Figure 9. a) Phagocytosis quantification using Incucyte live-cell analysis system on iMGL treated with pHrodo-labeled synaptosomes (syn). **b)** Fluorescent and brightfield microscopy of iMGL treated with pHrodo-labeled synaptosomes (syn) with/out cytochalasin D. **c)** Phagocytosis quantification using Incucyte live-cell analysis system on iMGL treated with pHrodo-labeled Aβ oligomer (Abo) and Aβ fibril (Abf). **d)** Fluorescent microscopy of iMGL treated with pHrodo-labeled Aβo with/out cytochalasin D and co-stained with 5-CFDA membrane marker.

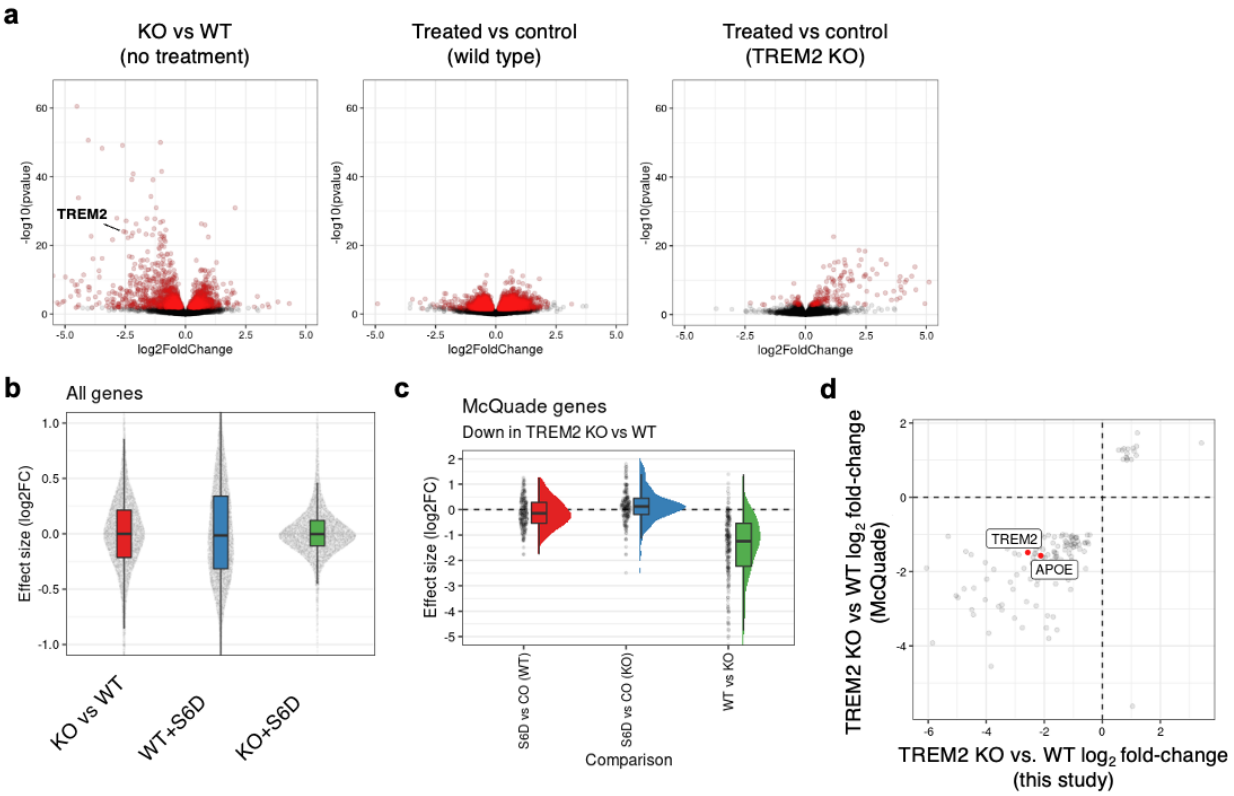

Supplementary Figure 10. a) Volcano plots for the differentially expressed genes in different iMGL RNA-seq experiments. Red genes correspond to differentially expressed at 10% FDR. **b)** Effect size distribution of the three iMGL experiments. **c)** Effect size distribution of downregulated genes in TREM2 KO iMGL from the McQuade et al. 2018 study in the three iMGL RNA-seq experiments. **d)** Comparison of reported effect sizes from the McQuade study and the TREM2 KO vs. WT iMGL RNA-seq experiment from this study.